

NASA Contractor Report 2951

NASA
CR
2951
c.1



LOAN COPY: RETURN TO
AFWL TECHNICAL LIBRARY
KIRTLAND AFB, N. M.

Effects of Grazing Flow on the Steady-State Flow Resistance and Acoustic Impedance of Thin Porous-Faced Liners

A. S. Hersh and B. Walker

CONTRACT NAS1-14310
JANUARY 1978

NASA



NASA Contractor Report 2951

Effects of Grazing Flow on the Steady-State Flow Resistance and Acoustic Impedance of Thin Porous-Faced Liners

A. S. Hersh and B. Walker
Hersh Acoustical Engineering
Chatsworth, California

Prepared for
Langley Research Center
under Contract NAS1-14310



National Aeronautics
and Space Administration

**Scientific and Technical
Information Office**

1978

TABLE OF CONTENTS

SUMMARY.....	1
1. INTRODUCTION.....	1
DEFINITION OF SYMBOLS.....	2
2. REVIEW OF D.C. AND A.C. IMPEDANCE PREDICTION MODELS...	5
2.1 D.C. Models.....	5
2.1.1 Linear Models.....	5
2.1.2 Nonlinear Models.....	9
2.2 Acoustic Models.....	10
3. STEADY-STATE FLOW RESISTANCE TESTS.....	17
3.1 Experimental Apparatus.....	17
3.2 Test Results.....	18
3.3 Derivation of Semi-Empirical Prediction Model....	19
4. ACOUSTIC IMPEDANCE TESTS.....	22
4.1 Two-Microphone Method and Test Set-up.....	22
4.2 Test Results.....	24
4.3 Derivation of Non-Grazing Flow Impedance Prediction Model.....	26
5. CONCLUSIONS.....	29
5.1 Steady-State Flow Resistance.....	30
5.2 Acoustic Impedance.....	30
REFERENCES.....	32
TABLES.....	34
FIGURES.....	40
APPENDIX A - Correction to Measured Incident Sound Pressure Level Due to Acoustic Radiation From the Test Specimen.....	72

SUMMARY

The results of an investigation of the effects of grazing flow on the steady-state flow resistance and acoustic *impedance* of seven Feltmetal and three Rigimesh thin porous-faced liners are presented. A state-of-the-art review of previous nongrazing flow studies is also presented. The steady-state flow resistance of the ten specimens were measured using standard fluid mechanical experimental techniques. The acoustic impedance was measured using the two-microphone method. The principal findings of the study are (1) the effects of grazing flow were measured and found to be small, (2) small differences were measured between steady-state and acoustic resistance, (3) a semi-empirical model was derived that correlated the steady-state resistance data of the seven Feltmetal liners and the face-sheet reactance of both the Feltmetal and Rigimesh liners.

These findings suggest that nongrazing flow steady-state flow resistance tests could provide considerable insight into the acoustic behavior of porous liners in a grazing flow environment.

1. INTRODUCTION

Sound absorbent treatments consisting of cavity-backed porous faced liners are currently being used to control internally generated machinery noise. For application to the inlet and exhaust ducting of jet engines, the efficient design of the liner should incorporate the effects of both high grazing flow velocities and intense sound pressure levels. Unfortunately, there have been few investigations of the effects of grazing flow and sound pressure on the relationship between the liner impedance and its construction (i.e., sheet thickness, porosity, fiber diameter, etc). The purpose of this report is to describe the results of a fundamental investigation of the effects of grazing flow and sound pressure on the steady-state flow resistance (herein referred to for brevity as d.c. resistance) and the specific acoustic impedance (i.e., resistance and reactance) of ten cavity-backed porous-faced specimens. The acoustic measurements were made using the two-microphone method. This method was used by Hersh and Walker¹ to study the effects of grazing flow and sound pressure level on the impedance of isolated orifices.

Feder and Dean² studied experimentally the effects of grazing flow and sound pressure on the d.c. resistance and acoustic impedance of a variety of acoustic liner configurations including porous-faced liners. The acoustic measurements were conducted using an impedance tube. They concluded that the d.c. and a.c. resistance increased and the reactance decreased with increasing grazing flow velocity and sound pressure level. The correlation between the d.c. and a.c. resistance for three porous-faced materials at a fixed grazing flow speed and sound pressure level was found to be generally poor; the a.c. resistance values were consistently higher (e.g., an a.c. value of 600 rayls vs. a d.c. value

of about 370 Rayls for a Feltmetal specimen) than the corresponding d.c. values. Feder and Dean did not interpret their results physically.

P. Dean³ used the two-microphone method to measure the effects of grazing flow on the impedance of cavity-backed perforates and porous faced liners. His results were in contrast with Feder and Dean's results in that the acoustic resistance of some materials did not change while other *decreased* with increasing grazing flow; the reactance *increased* with increasing grazing flow. Dean offered no explanation. Plumblee, et. al⁴ also investigated experimentally the effects of grazing flow on porous-face materials using the two-microphone method. Since the grazing flow speeds never exceeded 15 m/sec., they found no significant change in impedance. None of these studies investigated the nonlinear behavior of porous-faced materials.

The present understanding of the connection between porous material properties and a.c. and d.c. impedance for nongrazing flow is reviewed in Section 2. The results of an experimental and analytical investigation of the d.c. resistance and the a.c. impedance of ten porous-faced liners are described in Section 3 and 4 respectively. The major findings of the report are summarized in Section 5.

DEFINITION OF SYMBOLS

<u>Symbol</u>	<u>Definition</u>
A	cross-section area, (meter ²)
a	average spacing between fissures (meters); also constant
b	average slit height of fissure (meters); also constant
c	speed of sound (meters/second)
c _f	skin friction coefficient
c ₀	numerical coefficient (see Eq. 9)
C _D	drag coefficient
D	diameter of porous specimen (meters); also drag (Newtons)
f	frequency (Hz)
g	gravitational constant (meters/seconds ²)
H	height of duct containing specimen (meters)
h	complex wave number within porous material (meters ⁻¹)

<u>Symbol</u>	<u>Definition</u>
k	material permeability constant (meters ²)
K	material hydraulic conductivity constant (meter/second); also compressibility modulus ($= \frac{1}{\rho_0} \partial \rho' / \partial p'^{-1}$ / Newtons/meters ²)
L	thickness of porous specimen (meters); also length scale characterizing interaction between cylinders (meters); also depth of cavity (meters)
L _{ch}	length scale characterizing thickness of unsteady viscous layer (meters)
m	material structure factor (ratio of effective density of the air in the pore space to the actual density ρ_0 of the air)
M	material specific internal area (meters ⁵)
N	number of fibers or capillaries
P _s	static pressure upstream of specimen (Newtons/meter ²)
P _∞	static pressure in test section (Newtons/meter ²)
P _T	total pressure in test section (Newtons/meter ²)
P	material porosity
p	steady-state pressure (Newtons/meters ²)
p'	acoustic pressure (Newtons/meters ²)
Δp	pressure drop across specimen (N/m ²)
Q	volume flow, (meters ³ /second)
R	average hydraulic radius (meters)
R _{ac}	acoustic resistance (Rayls-mks)
R _{dc}	steady-state flow resistance (Rayls-mks)
R _e	Reynolds number
r	radial distance (meters)
S	spacing between cylinders (meters)
t	time(seconds)
T	material tortuosity
u	longitudinal component of velocity (meters/second)
V _∞	test section speed (meters/second)
V	volume of cavity (meters ³)

<u>Symbol</u>	<u>Definition</u>
V_D	average flow speed incident to porous material (meters/second)
v_x', v_y'	acoustic velocity (meters/sec)
X	reactance (Rayls-mks)
x	axial and/or longitudinal coordinate (meters)
y	normal and/or lateral coordinate (meters)
W	width of test section containing specimen (meters); characteristic (complex) impedance of porous material (Rayls-mks)
ϵ	constant defined by Eq. (46)
α	constant; also attenuation constant (meters^{-1})
$\alpha(\delta)$	probability distribution function
β	constant; also phase constant (degrees/meters)
δ	average cylinder diameter (meters); also average pore diameter (meters)
Γ	parameter defined by Eq. (26)
ρ, ρ'	steady-state and acoustic density (kilograms/meters ³)
Ψ	velocity potential ($\text{meters}^2/\text{second}$)
γ	ratio of specific heat of air
τ	material thickness (meter)
τ_w	wall shear stress (Newtons/meter ²)
λ	sound wavelength (meters)
ϕ	phase change across specimen (degrees)
μ	fluid coefficient of viscosity (kilograms/second/meter)
ν	fluid kinematic viscosity ($\text{meters}^2/\text{second}$)
ω	radian frequency (Hz)
κ	effective compressibility of the air within the porous material (Newtons/meters ²)

Subscripts

$()_o$	denotes open quantity
$()_c$	denotes closed quantity
inc	incident
cav	cavity
s	along stream tube direction
t	face-sheet

Superscripts

Definition

()' denotes acoustic quantity

2. REVIEW OF D.C. AND A.C. IMPEDANCE PREDICTION MODELS

In contrast to the sparse number of investigations of the effects of grazing flow on the d.c. and a.c. impedance of porous-faced materials, there have been a large number of investigations of their nongrazing flow behavior. A review of the more important papers is given below to provide background information necessary to place in perspective the results of the present investigation. The d.c. models are described in Section 2.1 followed by the a.c. models in Section 2.2.

2.1 D.C. Models

The review of the d.c. resistance models is divided into linear and nonlinear parts. The linear models represent variations and/or refinements of Darcy's Law⁵. Darcy was the first to establish a linear connection between the deriving pressure gradient Δp across a porous specimen and the average flow speed V_D approaching the specimen. For sufficiently high average speeds, the connection between Δp and V_D is nonlinear due to a quadratic relation between Δp and V_D . Most of the details of the various models described below are based on the excellent review by Bear⁶.

2.1.1 Linear Models

In 1856 Darcy investigated the flow of water in vertical homogeneous sand filters in connection with the fountains of the city of Dijon, France. From his experiments, he concluded that the volume rate of flow Q through the filter was proportional to the product of the cross-sectional area of the filter A and the pressure difference across it (Δp) and inversely proportional to the filter length (L) leading to the relationship

$$Q = K A \left[\frac{(\Delta P / \rho g)}{L} \right] \quad (1)$$

where the constant K is called the material hydraulic conductivity, ρ is the density of the water and g is the gravitational constant. Later researchers separated the influence of the material from that of the fluid by defining $K = \rho g k / \mu$ where μ is the viscosity of the fluid and k is the specific permeability of the porous material. Substituting this expression for K into Eq. (1) yields the modern form of Darcy's Law,

$$V_D = \frac{k}{\mu} \left(\frac{\Delta P}{L} \right) \quad (2)$$

where V_D is the average flow speed approaching the porous material.

A particularly attractive and straight-forward application of Darcy's Law is to model a porous material as a collection of straight capillary tubes. Applying Hagen-Poiseuille's law to the flow through a capillary tube of radius δ , Scheidegger⁷ derived the following connection between V_D and Δp ,

$$V_D = \frac{\delta^2}{32\mu} \frac{\Delta p}{L} \quad (3)$$

Comparing Eqs. (2) and (3), the permeability constant $k = \delta^2/32$ for a capillary tube. If there are N tubes per unit cross-section of the model (normal to the direction of flow) then the porosity $P = N(\pi\delta^2/4)$ and the filter speed through the porous material is

$$V_D = \sum_{i=1}^N V_{D_i} = \sum_{i=1}^N \frac{\pi\delta^4}{128\mu} \left(\frac{\Delta p}{L} \right) = \frac{N\pi\delta^4}{128\mu} \left(\frac{\Delta p}{L} \right) = \frac{P\delta^2}{32\mu} \left(\frac{\Delta p}{L} \right); k = \frac{P\delta^2}{32} \quad (4)$$

What is important in Eq. (4) is that the filter speed is proportional to the product of the square of the average tube diameter δ^2 and the material porosity P ; the coefficient $1/32$ is obviously unimportant.

Scheidegger generalized the capillary model described above by replacing the porous material with a distribution of capillaries of different diameters. He introduced the quantity $\alpha(\delta)d\delta$ to represent the fraction of capillaries having radii between δ and $\delta+d\delta$. Assuming that the volume occupied by these capillaries parallel, say, to the x_i direction, is $1/3P\Delta x_i\alpha(\delta)d\delta$ per unit cross-section, the average filter speed $V_{D_{x_i}}$ is

$$V_{D_{x_i}} = \frac{1}{3} P \int_0^\infty V_{D_{x_i}}(\delta) \alpha(\delta) d\delta = \frac{P}{96\mu} \left(\frac{\Delta p}{L} \right) \int_0^\infty \delta^2 \alpha(\delta) d\delta \quad (5)$$

where $V_{D_{x_i}}(\delta)$ is the average speed in the capillaries of diameter δ given by Eq. (3). Comparing Eqs. (5) and (2) yields for the permeability constant

$$k = \frac{P}{96} \int_0^\infty \delta^2 \alpha(\delta) d\delta \quad (6)$$

Scheidegger also generalized the above model by permitting the capillary tubes to be tortuous (i.e., non-straight) and of variable diameter. He proposed the following expression for k ,

$$k = \frac{P}{96T^2} \left/ \left[\int_0^\infty \delta^2 \alpha(\delta) d\delta \right]^2 \int_0^\infty \frac{1}{\delta^6} \alpha(\delta) d\delta \right. \quad (7)$$

Here T is the "tortuosity" factor defined as the ratio of the length of the actual flow to the thickness of the porous material.

Irmay⁸ applied the capillary model to predict the resistance of narrow fissures (i.e., slits of constant width), a fractured rock being the closest application of his approach. Irmay derives the following expression for the permeability,

$$k = a^2 P^3 / 12 (1-P)^2 = Pb^2 / 12 \quad (8)$$

where b is the average slit height of the fissure and a is the average spacing between fissures. Here the material porosity $P = b/(a+b)$.

In 1927, Kozeny⁹ applied the concept of hydraulic radius R to connect the permeability constant k to the material properties. Defining R as the ratio of volume of a conduit to its wetted surface area, he derived $R = P/M$, where M is the specific surface area of the porous material. Using this definition, R may be interpreted as the average hydraulic radius of quite complicated flow channels. By solving the Navier-Stokes equations for all channels passing through a cross-section normal to the flow, Kozeny derived the following expression for the material permeability constant k ,

$$k = c_0 P^3 M^2 / (1-P)^2 \quad (9)$$

where c_0 is a numerical coefficient called Kozeny's constant ($c_0 = 0.5, 0.562, 0.597, 0.667$ for a circle, square, equilateral triangle, and rectangle respectively).

Recently theoretical estimates of the permeability constant have been derived using a drag model. The idea here is that the pressure drop through a material is related to internal shear (tangential) and normal (pressure) stresses by assuming that a porous material can be modelled as a collection of closely packed

spheres. For example, Rumer and Drinker¹⁰ and later Rumer¹¹ derived the following expression for the material permeability constant,

$$k = \frac{\beta P^2 d^2}{\lambda(1-P)} \left(\frac{\Delta p}{L} \right) \quad (10)$$

where d is the porous material average diameter, λ is a coefficient that takes into account the effects of neighboring spheres (for a single sphere in an infinite fluid $\lambda = 3\pi$) and β is a shape factor ($\beta = \pi/6$ for a sphere).

Iberall¹² assumed that highly porous materials could be modelled as a collection of randomly orientated circular cylindrical fibers of the same diameter. He then derived an expression for the material permeability by assuming that the pressure drop necessary to overcome the viscous drag is linearly additive for all of the fibers. The idea here is that the average speed is sufficiently low, the pressure drop across the material is equal to the viscous drag of the fibers. Since Iberall ignored interactions between fibers, his analysis is restricted to large separation distances between fibers and hence to high porosity materials.

Iberall assumed that given n fibers of unit length per unit volume, $n/3$ of them will be orientated perpendicular to the local upstream velocity V_D . Using Lamb's¹³ calculation of the drag per unit length for a cylinder perpendicular to a stream, Iberall derived the following expression for the pressure drop across a specimen

$$\frac{\Delta p}{L} = \frac{16\mu V_D (1-P)}{3P\delta^2} \cdot \frac{4 - \ln(Re)}{2 - \ln(Re)}; \quad Re = V_D \delta / \nu \quad (11)$$

where δ is the average radius of the fibers. Comparing Eqs. (11) and (21) the permeability k is

$$k = \frac{3P\delta^2}{16(1-P)} \cdot \frac{2 - \ln(Re)}{4 - \ln(Re)} \quad (12)$$

Equation (12) is unusual because it shows that the material permeability is not only a function of the material properties but is also a function of the fluid inertia through the Reynolds number. Scheidegger⁷ suggests that the drag theory may represent a generalization of Darcy's Law.

2.1.2 Nonlinear Models

For the linear relationship between Δp and V_D to be valid, the Reynolds number characterizing the flow through the porous material must be extremely small. As used here, the Reynolds number is defined as $Re = V_D \delta / \nu$ where V_D/P is the average velocity in the material and δ the average pore diameter of the material. The Reynolds number can be interpreted as a measure of the relative importance between inertia and viscous forces. To show this, consider flow over an isolated cylinder of radius δ . By nondimensionalizing all length changes by the cylinder diameter δ and all velocity changes by the *local* upstream velocity V_D/P , it follows that the order-of-magnitude of a typical nonlinear term $\rho u \partial u / \partial x$ is $(\rho / \delta) (V_D/P)^2$ and that the order-of-magnitude of a typical shear stress term is $\mu \partial^2 u / \partial y^2 \sim \rho V_D^3 / \nu P^3$. The ratio of the nonlinear inertial to viscous terms is $V_D \delta / \nu = Re$.

It is clear that the flow within a porous material cannot be accurately modelled by a collection of straight, constant area, capillary tubes. A more realistic model would have to incorporate both twisting fully three-dimensional motion with the fluid accelerating and decelerating within the material. Recognizing this Scheidegger believes that the onset of nonlinearity first occurs due to *laminar* flow turning and fluid accelerations and decelerations. At higher speeds, nonlinear losses arise due to *turbulence* generated within the porous material. According to the review by Bear, initial deviations from Darcy's linear law occur for Reynolds number as low as $Re = 0.1$. The deviations increase for increasing Reynolds number. These deviations are believed to arise from the onset of laminar nonlinearity as discussed above. The onset of turbulence generated nonlinearity does not occur until Reynolds numbers between 60 to 150. In general, the following relationship between Δp and V_D characterize the d.c. resistance,

$$\Delta p = a V_D + b V_D^2 ; a, b \text{ constants} \quad (13)$$

Here a is proportional to μ and independent of the fluid density ρ and b is proportional to ρ and independent of μ .

Blick¹⁴ analyzed the nonlinear behavior of porous materials in a rather interesting way. His model consisted of a bundle of capillary tubes with orifice plates spaced along each tube, separated by a distance equal to the mean pore diameter. Assuming the fluid is homogeneous, Newtonian and one-dimensional, Blick derives the following expression relating p and V_D .

$$-\frac{\partial p}{\partial x} = \left[\frac{2c_f \text{Re}\mu}{P\delta^2} \right] V_D + \left[\frac{C_D \rho}{2\delta P^2} \right] V_D^2 \quad (14)$$

where c_f is the skin friction coefficient of the flow along the tube walls of constant diameter δ , $\text{Re} = V_D \delta / \nu$ is the diameter based Reynolds number and C_D is the drag coefficient of the orifice plate. Blick's model is important because it shows qualitatively the nature and form of nonlinear pressure losses. For a detailed discussion of other models, the reader is referred to the review by Bear.

This review of flow nonlinearity concludes by quoting from Bear's review. "*Cheaveteau and Thirriot*¹⁵ perform experiments in several two-dimensional models that permit visual observations of streamlines and streaklines. In a typical model, which has the shape of a conduit that diverges and converges alternately, they observe streaklines. For $\text{Re} < 2$, the flow obeys Darcy's law and the streamlines remain fixed. As Re increases, streamlines start to shift and fixed eddies begin to appear in the diverging areas of the model. They become larger as Re increases. At $\text{Re} = 75$ turbulence appears and starts to spread out as Re increases. Turbulence covers some 50% of the flow domain at $\text{Re} = 115$ and 100% of it at $\text{Re} = 180$. The deviation from Darcy's law is observed at $\text{Re} = 2-3$. Thus the deviation from Darcy's law as the velocity increases is associated with gradual shifting of streamlines due to the curvature of the microscopic solid walls of the pore space."

2.2 Acoustic Models

Despite widespread application of porous materials as sound absorbers, surprisingly little *fundamental* research has been conducted in the past twenty years to understand their acoustic behavior. Most of the recent research has been applications oriented in the sense that existing parameters used to define the important physical properties, namely structure factor, bulk modulus of compressibility and dynamic flow resistance are measured or assumed known. The results of three investigations are reviewed below representing the pioneering work of Scott¹⁶, Zwicker and Kosten¹⁷ and Morse¹⁸. These three are believed to adequately summarize the state-of-the-art. None of the investigators considered the acoustic nonlinear behavior of porous materials.

Scott was one of the first to be concerned with the propagation of acoustic disturbances in porous materials. He assumed the porous material to be homogeneous, isotropic and sufficiently large in extent so that reflected waves were negligible. He

further assumed that the porous material consisted of very many small fibers or particles packed together so as to leave between them interconnected air-spaces or pores of irregular shape. Defined in this way, the linearized equations of motion for sound waves propagating through the pore space are obtained. The linearized conservation of momentum equation becomes

$$-\nabla p' = m\rho_0 \frac{\partial}{\partial t} \left(\frac{\vec{V}_D}{P} \right) + R_{a.c.} \vec{V}_D \quad (15)$$

where m is the ratio of the effective density of the air in the pore space to the actual density ρ_0 of the air (called the structure factor by other investigators), p' is the acoustic pressure, $R_{a.c.}$ is a dynamic resistance constant analogous to the d.c. resistance used in Darcy's law, P is the material porosity and \vec{V}_D is the vector velocity approaching the porous material. The corresponding linearized mass conservation equation is given by

$$\frac{\partial \rho'}{\partial t} + \rho_0 \nabla \cdot \left(\frac{\vec{V}_D}{P} \right) = 0 \quad (16)$$

By introducing the acoustic velocity potential $\vec{V}_D = \text{grad } \psi$, Scott derives the following linearized wave equation

$$\nabla^2 \psi + h^2 \psi = 0 \quad (17)$$

with

$$h^2 = \frac{m\rho_0 \omega^2}{\kappa} - \frac{i R_{a.c.} P \omega}{\kappa} \quad (18)$$

The quantity h is the complex propagation constant within the material and κ is the effective compressibility of the air in the pore spaces. By introducing the complex density ρ' defined as

$$\rho' \equiv \frac{h^2 \kappa}{P \omega^2} \quad (19)$$

Scott derived the wave equation in a form similar to the wave equation in free space. The remainder of his paper describes the use of a probe tube to measure the real and imaginary parts of the propagation constant h . Writing $h = \beta - i\alpha$, the decay of intensity with distance provides a measurement of the attenuation constant α . The corresponding change in phase of the acoustic pressure with distance provides a measurement of the wavelength, and therefore of β . With h specified, the complex density ρ' follows immediately from Eq. (19).

Scott compares his theory with measurements of a variety of rock-wool porous samples of different thicknesses. At $f = 200$ Hz, he concludes that for a rock wool sample, the effective density of the air trapped within the pores was roughly twice its free air value; it decreased to about 1.32 at $f = 4000$ Hz. His measurements also showed that at $f = 200$ Hz, the dynamic resistance was equal to its d.c. value. The speed of sound varied from c_0/γ at low frequencies to c_0 at the higher frequencies, thus indicating that low frequency sound propagates isothermally and high frequency adiabatically. Scott's paper is obviously important. His desire to recast the sound propagation equations in a form equivalent to that in free space is understandable. Unfortunately, in the process of forcing the analogy, he as well as Zwikker and Kosten may have induced workers in the field into believing that the effective mean density of sound waves propagating in porous materials is a function of the structure factor m , porosity P , flow resistance $R_{d.c.}$ and frequency ω . In reality the mean density of the air is constant since the air can be considered incompressible. While m , P , r and ω affect the sound pressure, density and velocity, they do not affect mean density. This is most evident at low frequencies where the a.c. resistance is equal to the d.c. flow resistance. At the low particle speeds, generated by the sound waves, the incident sound driving pressure cannot increase the air-density - clearly the process is incompressible. Thus interpretations other than increases in the fluid mean density are required.

In 1949, Zwikker and Kosten published their famous book entitled, Sound Absorbing Materials, which dealt in part with the connection between the quantities h and ρ' and the material structural properties. Zwikker and Kosten (herein referred to as Z & K) introduced the following assumed solution describing the propagation of a plane sound wave in a homogeneous isotropic medium extending to infinity,

$$p'(x, t) = A e^{-\alpha x + i(\omega t - \beta x)} \quad (20)$$

where α is the attenuation constant of the sound wave, $\beta = \omega/c$ is the corresponding phase constant (c is the phase velocity of the sound wave in the material) and A is an arbitrary amplitude. A second constant is defined, called W , the characteristic (complex) impedance of the infinite extent material, $W = p'(x,t)/v_x'(x,t)$. Here $v_x'(x,t)$ is the sound particle speed in the x - direction within the material. W is defined as $\sqrt{1/\rho_0 K}$ where $K = (\partial p'/\partial \rho')/\rho_0$ is related to the complex speed of sound in the material. W is complex due to internal material damping of the propagating sound wave; it denotes that acoustic density variations within the material are not in phase with the driving pressure variation. There are two limiting cases in which p' and ρ' vibrate in phase with other. In the first limit, the sound frequency is sufficiently low that the transmission of heat to and from the solid frame is rapid enough so that the enclosed air is kept at constant temperature (isothermal case). At high frequencies, the transmission of heat is so slow that the air vibrates adiabatically. Between these limits hysteresis, occurring between the instantaneous heating and cooling of the air by the sound field and the subsequent transfer of heat to and from the material, results in a frequency dependent complex propagation constant.

The continuity and momentum conservation equations governing the motion of the sound waves are, respectively,

$$-\frac{\partial v_x'}{\partial x} = \frac{P}{\rho_0} \left(\frac{d\rho'}{dp'} \right) \frac{\partial p'}{\partial t} \quad \text{and} \quad \frac{\partial p'}{\partial x} = \left(\frac{m}{P} \rho_0 \right) \cdot \frac{\partial v_x'}{\partial t} + R_{a.c.} v_x' \quad (21)$$

where P is the material porosity, $R_{a.c.}$ the material a.c. resistance and m the structure constant. For low frequency oscillations ($\sqrt{\omega \delta^2/\nu} \ll 1$) $R_{a.c.} \approx R_{d.c.}$. The quantity $R_{d.c.}$ follows from Poiseuille's law governing the behavior of steady-state flow in capillary tubes, namely

$$R_{d.c.} = 8 m \mu / P \delta^2 \quad (22)$$

where δ is the average material pore radius. For high frequency oscillations ($\sqrt{\omega \delta^2/\nu} \gg 1$),

$$R_{a.c.} \approx \frac{m}{P} \frac{1}{r_0} \sqrt{2 \mu \omega \rho_0} \quad (23)$$

Z & K offer the following interpretation of the term m/P that multiplies the density ρ_0 of the free air in the momentum equation. They split the factor into two parts, m and $1/P$. The quantity m is thought to consist of two parts, one of which is related to the internal friction of the air, the other to the orientation of the material pores. A third part also exists, the inertia of the structural material, but Z & K feel that in most cases this effect is small.

Of the various contributors to m the pore orientation is the most important. Z & K show that it contains the factor $(1/\cos^2\theta)$. For randomly orientated pores $m \approx 3$. According to experiments, m has values lying between 3 and 7. By introducing the apparent (complex) density defined as

$$\rho' = \frac{m}{P} \rho_0 - \frac{iR_{d.c.}}{\omega} , \quad (24)$$

the equations of motion for a traveling wave is brought into the universal form,

$$\Gamma p' = i\omega \rho' v_x' \quad (25)$$

where

$$\Gamma = i\omega \sqrt{\rho'/\kappa} , \quad W = \sqrt{\kappa \rho'} \quad (26)$$

Zwikker and Kosten's book is an accurate state-of-the-art summary of the acoustical understanding of porous materials through 1949. Following Scott, the authors chose to cast the form of the equations of motion into a universal form - i.e., similar in form to the equations of motion describing the propagation of sound in air. Thus their interpretations suffer the same limitations as those of Scott.

Morse extends the approach adopted by Zwikker & Kosten (first presented by Rayleigh)¹⁹ and by Scott, Morse and Bolt²⁰, Beranek²¹ & others to model the propagation of sound in granular media. He assumes that all of the grains have roughly the same diameter. He derives the following equations governing the sound motion in the granular material,

$$\rho_o \nabla \cdot \tilde{v}' = -P \frac{\partial \rho'}{\partial t}$$

$$\rho' = c_o^2 \rho'$$

(27)

$$-\nabla p' = \left(\frac{m}{P}\right) \rho_o \frac{\partial \tilde{v}'}{\partial t} - R_{d.c.} \tilde{v}'$$

Here \tilde{v}' is volume of fluid per unit area in direction pressure gradient

ρ', ρ_o are the acoustic and equilibrium fluid density respectively

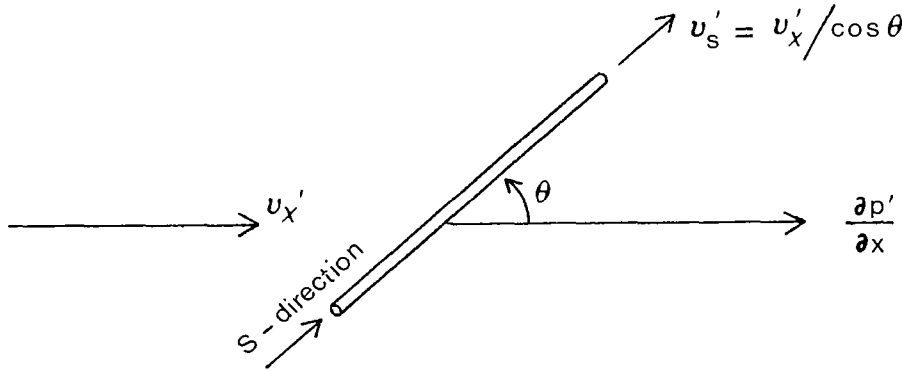
p' is the excess instantaneous pressure

m is the structure factor (explained below)

P is the material porosity

R_{dc} is the dynamic flow resistance

Morse defines the structure factor m as arising because of the way in which the solid material constrains the motion of the fluid. Not all the fluid is in the direction of the pressure gradient $\nabla p'$. To explain this, consider small tubes inclined at an angle θ to the pressure gradient,



In the S-direction (along the tube), the momentum equation is

$$\rho_o \frac{\partial v_s'}{\partial t} = -\frac{\partial p'}{\partial s} \quad (28)$$

Now $u_s' \cos \theta = u_x'$ and $s \cos \theta = x \rightarrow \partial / \partial s = \cos \theta \partial / \partial x$. Thus substitution yields

$$\left(\frac{1}{\cos^2 \theta}\right) \cdot \rho_o \frac{\partial v_x'}{\partial t} = -\frac{\partial p'}{\partial x} \quad (29)$$

Averaging the tubes over all possible angles assuming that all the tubes are orientated uniformly in direction, the probability that a given tube lies between the spherical angles θ , $\theta+d\theta$ and ϕ , $\phi+d\phi$ is unity, then

$$\langle \cos^2 \theta \rangle = \frac{1}{2\pi} \int_0^{2\pi} d\phi \int_0^{\pi/2} 1 \cdot \cos^2 \theta \cdot \sin \theta d\theta = 1/3$$

Thus, $m=3$. Morse does not allow for inertial coupling between the *motion* of the porous material and its effect on the air.

Assuming a plane wave solution of the form $p'(x,t) \sim e^{i(\omega t - kx)}$ Morse shows that $k = (\omega/c_o) \sqrt{m - iR_{dc}P/\rho_o \omega}$. Assuming further that $R_{dc}P/\rho_o \ll 1$, the propagation constant k may be written

$$k \simeq \sqrt{m} \frac{\omega}{c_o} - i R_{dc} P / 2 \rho_o c_o^2 \sqrt{m} \quad (30)$$

Thus the absorption (α) and sound propagation speed (c) within the material follows immediately to be

$$\alpha \simeq R_{dc} P / 2 \rho_o c_o^2 \sqrt{m} \quad (31)$$

$$c = c_o / \sqrt{m}$$

Clearly, the structure factor $m(m>1)$ as defined above results in a reduced sound propagation speed. Obviously m includes heat transfer effects (isothermal, adiabatic) not explicitly discussed by Morse.

Morse proceeds to connect the dynamic resistance R_{dc} to the known acoustic behavior in small tubes. At low frequencies where the acoustic Reynolds number $R_a = \sqrt{\omega \delta^2 / \nu} \ll 1$, $R_{dc} \simeq R_{ac} = 8\nu m / P \delta^2$. Inserting R_{dc} into Eq. (31) shows that $\alpha \sim \sqrt{m}$. At high frequencies where $R_a \gg 1$, $R_{ac} = m \sqrt{2\mu\omega\rho_o} / P \delta$. The absorption α is also proportional to \sqrt{m} . Morse concentrates only on the high frequency case. He analyses available data to show that $\alpha \sim \sqrt{\nu R_{dc}}$.

Morse's paper is attractive because he does not identify the quantity m/P as increasing the effective density of the air trapped within the porous material as do Scott and Z & K. Instead, he interprets m to affect the magnitude of the pressure gradient because of lateral fluid motion induced by the structure not in the direction of the pressure gradient. The porosity P is obvious and requires no explanation. Morse interprets the effective speed of sound c in the material to be $c=c_0/\sqrt{m}$ where c_0 is its adiabatic value in free air (recall that Morse considers only the high frequency solution). While this interpretation is valid at high frequencies, it is incorrect at low frequencies wherein c_0 should be redefined as c_0/γ (the isothermal sound speed).

3. STEADY-STATE FLOW RESISTANCE TESTS

Many investigators have shown that in the absence of grazing flow, the d.c. and a.c. resistances of porous materials are equal (e.g., see the study by Zorumski and Parrott²²). For application to the aircraft industry, it is of interest to determine whether this equivalency is still valid in the presence of a grazing flow. Accordingly, d.c. flow resistance tests were conducted with the porous-faced liner specimens.

Table I summarizes the manufacturers' predicted acoustic properties. Specimens #1-7 were made from Feltmetal fiber metals and specimens #8-10 from Rigimesh stainless steel wire cloth. Photographs enlarged to illustrate the detailed structure of typical Feltmetal and Rigimesh specimens are shown in Fig. 1.

3.1 Experimental Apparatus

The effects of grazing flow were studied experimentally in the HAE wind tunnel shown in Figure 2. The test section, made from .0127 meters thick transparent acrylic sheet, has a removable side-wall containing the test specimen. The porous test material was backed by a cylindrical tube of diameter .0508 meters; it was secured and flush mounted to the test section side wall by means of three set screws. Flow through the side branch was controlled by means of blowers used in the suction mode (i.e., from the test section into the side branch) or blowing mode (i.e., from the side branch into the test section). The side branch volume flow rate was monitored by means of sharp-edge orifices. By accurately measuring the pressure drop across the orifices with Charles Merriam Company calibrated slant manometers, volume flow rates as low as 8.5×10^{-5} cubic meters per second were recorded.

Test section speeds up to 91.44 meters/second were measured. The velocity profile for $V_\infty=85.6$ meters/second, is shown in Figure 3. As shown, the boundary layer is turbulent - measurements

showed it to be turbulent for all test speeds considered. For distances less than .00051 meters from the tunnel wall, the data indicates that the flow is separated due to interaction between the boundary layer probe and wall. The data matches closely the classical 1/7th velocity law profile for .00051 meters < y < .00762 meters.

The d.c. resistance R of a typical specimen mounted as shown in the lower part of Figure 2 is defined as the ratio of the pressure drop ΔP across the material to the average (within the .0508 meter diameter tube) velocity V_D ,

$$R_{d.c.} = \frac{\Delta P}{V_D}$$

The pressure drop was measured directly from a calibrated Charles Merriam slant manometer. The average speed was calculated using standard ASME techniques²³ from the pressure drop measurements across the orifices (orifice diameters of .00635 meters, .0127 meters and .01905 meters were used to extend the useful range of V_D from a minimum of .04 to a maximum of 10 meters/second).

3.2 Test Results

Figures 4-9 summarize the effects of grazing flow on the d.c. flow resistance of the ten specimens operating in both the suction and blowing mode. In agreement with the discussion preceeding Eq. (13), the data can be accurately presented by the empirical curve fit

$$R_{d.c.} = \frac{\Delta P}{V_D} = a + b V_D \quad (32)$$

The various measured values of a and b are tabulated in Table II. Inspection of Table II shows that, in general, there are only small differences between the blowing and suction data. Further, the effects of grazing flow are also shown to be small. Most of the differences are of the order of 20% or less. These differences are considered small relative to the effects of grazing flow on the d.c. resistances of orifices as measured by Feder and Dean.

The measured negligible differences in flow resistance for the specimens operating in the blowing and suction modes indicate that the material permeability is isotropic in the axial direction. Flow nonlinearity is shown to become important for $V_D > 2$ meters/second for specimens 2, 3, 4, 8, 9 and 10 for $V_D > .30$ meters/second for specimens 1, 5, 6 and 7 (recall from Table I that these

specimens should be equivalent). This is reflected in the various values of the coefficient b summarized in Table II. Since b is a measure of the importance of flow nonlinearity, following the arguments of Scheidigger, it is a function of the area changes associated with the various pore diameters. The idea here is that relatively large pressure gradients are required to balance the relatively large convective velocity gradients which arise from abrupt changes in internal pore diameter cross-sectional areas.

Specimen 1, 5, 6 and 7 should, in principle, exhibit roughly the same steady-state flow resistance behavior. Clearly, the data characterizing specimens 5 and 6 are reasonably close - the coefficients a and b are within 20%. The corresponding coefficients characterizing specimens 1 and 7, however, are quite different. These differences are probably associated with the variability inherent with their manufacture. The details of this variability are not well understood nor documented.

The negligible changes in flow resistance with grazing flow require special comment. A small positive pressure drop $\Delta P_S = P_S - P_\infty$ induced across the specimen by the grazing flow was observed. The flow control valves across the side branch were closed so that there was zero mean flow across the specimen. According to the investigations by first Beavers and Joseph²⁴ and later Taylor²⁵, the observed pressure drop arises because of a local recirculating (vortical) flow induced across the specimen. A sketch showing the vortical flow pattern is shown in Fig. 10. The recirculating flow is driven and maintained by steady-state shear stresses transferred across the porous surface. Figure 11 shows the effect of correcting the data by subtracting this pressure drop from the measured blowing data (adding for the suction data) for the data of Specimen #4. Without this correction, the flow resistance would increase without limit as $V_D \rightarrow 0$ as indicated in Fig. 11 (in the suction mode, it would decrease without limit). Table III summarizes the measured pressure drops ΔP_S in meters of water across the ten specimens at a grazing flow speed of $V_\infty = 79.6$ meters/second. The measurements showed that (ΔP_S) is linearly proportional to the test section head $(P_T - P_\infty)$ where P_T is the test section total pressure and P_∞ is the test section static pressure.

3.3 Derivation of Semi-Empirical Prediction Model

A simplified prediction model of the nongrazing linear d.c. resistance of thin porous-faced liners is derived. The intent here is to correlate the linear d.c. resistance data. It is understood because of the variations inherent in the manufacturing process that only an approximate correlation is possible. The photographs of the Feltmetal specimens, shown in Figure 1, suggest that

they can be modelled as a collection of small diameter cylinders. A model of the Rigimesh specimens will not be derived because of the very limited number of specimens supplied by the manufacturer. To simplify the model, the following assumptions are made. The cylinders have mean diameter δ . They are aligned perpendicular to the incident flow V_D as shown in Fig. 1. The specimen has zero thickness, that is, all the cylinders are assumed to lie on a plane surface - this treats the specimen surface as a momentum sink in a manner similar to that proposed by Zorumski and Parrott. The cylinders are separated by an average center-to-center spacing S as shown schematically in Figure 1. Here the specimen is placed in a duct of width W and height H with incident flow V_D as shown. The parameters H , N and δ are related as follows

$$H \simeq NS \quad \text{for } N \gg 1 \quad (33)$$

Consistent with the liner zero thickness assumption, the porosity P is defined as the ratio of the open area A_0 to the total area A_T ,

$$P \equiv \frac{A_0}{A_T} = 1 - N\delta W / HW \quad (34)$$

Substituting Eq. (33) into Eq. (34) and assuming N large yields the following approximate estimate of the porosity,

$$P \simeq 1 - \delta/S \quad (35)$$

The d.c. resistance is calculated by assuming that the cylinders act as a momentum sink. From momentum balance considerations, the following relationship exists between the pressure drop Δp across the specimen and the drag force due to the cylinders,

$$\Delta p \cdot HW = ND \quad (36)$$

where N is the total number of cylinders (of width W) and D is the drag force on each cylinder. Now assume for very slow upstream average speeds V_D , that the cylinder drag is proportional to the

skin friction shear stresses τ_w where

$$D = \tau_w \pi \delta W \sim \left[\frac{\mu (V_D/P)}{L_{ch}} \right] \pi \delta W \quad (37)$$

Here (V_D/P) is the local pore velocity incident to the cylinder and L_{ch} is a measure of the thickness of the viscous shear layer normal to the cylinder surface. For very low Reynolds number flows, the characteristic length L_{ch} for an isolated cylinder is the diameter δ . For collections of closely spaced cylinders, however, L_{ch} must be a function of the separation parameter S . Thus for $S/\delta \gg 1$, $L_{ch} = \delta$ and for $S/\delta < 1$, $L_{ch} = f(S/\delta)$. Here S/δ may be thought of as an interaction parameter. The following simplified empirical relationship is suggested,

$$L_{ch} \approx \frac{\alpha S}{1 + \alpha (S/\delta)} \quad (38)$$

For $S/\delta \gg 1$, $L_{ch} \approx \delta$. For $S/\delta \ll 1$, $L_{ch} \approx \alpha S$ where α is a constant that must be determined from experimental data. Hopefully, α will be independent of specimen geometry. Combining Eq. (37) and Eq. (38) and substituting into Eq. (35) yields

$$\Delta p \approx \frac{HD}{HW} \sim \frac{N\pi\mu V_D \delta WP}{HWP\alpha S} \left[1 + \alpha (S/\delta) \right] \quad (39)$$

Substituting Eqs. (33) and (34) into Eq. (39) and solving for the ratio $\Delta p/V_D$ yields

$$R_{d.c.} \equiv \Delta p/V_D \sim \frac{\pi\mu}{\alpha\delta} \left(\frac{1-P}{P} \right) \left[1 - P + \alpha \right] \quad (40)$$

The following form of the d.c. flow resistance model is written as

$$R_{d.c.} \approx \beta \left(\frac{\mu}{\delta} \right) \left(\frac{1-P}{P} \right) (1 - P + \alpha) \quad (41)$$

where α and β are unknown constants.

The results of applying Eq. (41) to determine the constants α and β are summarized in the fifth column of Table IV. The best

fit to the data occurred with $\alpha=0.8$; the average value of $\beta_{av}=1864$.

The model correlates the Feltmetal data quite well over a wide range of porosities (0.45 to 0.97), cylinder diameters (4×10^{-6} to 10^{-4} meters) and d.c. resistances (115 to 890 Rayls-mks). No particular significance is attached to the values of α and β . The porosity values shown in Table IV were estimated by computing the relative densities of the specimens. This involved subtracting out the weight of the screens and weighing the specimens and measuring their volume. The agreement between manufacturers estimated porosities and measured porosities are quite close.

No attempt was made to model the nonlinear behavior of the specimens. The reason for this is that specimens #2, 3 and 4 were just barely entering the nonlinear regime at the higher test filter speeds. Based on the flow visualization tests performed by Chauveteau and Thirriot (see Section 2.1), nonlinear deviations from Darcy's law were observed at values of Reynolds number $Re = V_D \rho / P_v$ between 2 and 3. Using these values of Re , the last column in Table IV shows the values of filter speed V_D corresponding to $Re=2$ and 3. Comparing these values with the observed values of V_D representing the onset of nonlinearity (the sixth column in Table IV) indicate fairly good agreement with Chauveteau and Thirriot's criteria. Accepting Chauveteau and Thirriot's criteria, it is clear that the onset of nonlinearity can be extended to very high average speeds V_D by using porous materials made of very small fiber diameters.

4. ACOUSTIC IMPEDANCE TESTS

In the previous section, the effects of grazing flow on the d.c. resistance of ten porous-faced materials were measured and found to be negligible. In this Section, the two-microphone method is used to measure the effects of grazing flow, sound pressure level and frequency on the acoustic resistance and reactance of the same ten specimens. The test apparatus and the two-microphone method is described in Section 4.1. The test results are summarized in Section 4.2. A non-grazing flow semi-empirical impedance prediction is derived in Section 4.3. The model is used to correlate the nongrazing test data of Section 4.2.

4.1 Two-Microphone Method and Test Set-up

The acoustic resistance, total reactance, and face-sheet reactance of the test specimens were measured using the two microphone method described by Dean³. The method requires the specimens to be cavity-backed. Figure 12 shows a schematic of the test set-up and the instrumentation used. The acoustic resistance and reactance of cavity-backed specimens can be

described by the following expressions

$$\frac{R}{\rho c} = \left[10^{\frac{\text{SPL (inc)} - \text{SPL (cav)}}{20}} \right] \frac{\sin \phi}{\sin\left(\frac{\omega L}{c}\right)} \quad (42)$$

$$\frac{X_f}{\rho c} = - \left[10^{\frac{\text{SPL (inc)} - \text{SPL (cav)}}{20}} \right] \frac{\cos \phi}{\sin\left(\frac{\omega L}{c}\right)} \quad (43a)$$

$$\frac{X_f}{\rho c} = \cot\left(\frac{\omega L}{c}\right) - \left[10^{\frac{\text{SPL (inc)} - \text{SPL (cav)}}{20}} \right] \frac{\cos \phi}{\sin\left(\frac{\omega L}{c}\right)} \quad (43b)$$

where $\text{SPL(inc)} - \text{SPL(cav)}$ represents the sound pressure level difference (in dB) between the incident and cavity sound fields and ϕ represents the corresponding phase difference. The quantities ω , L and c represent the sound radian frequency, cavity depth and fluid sound speed respectively. The above measurements are obtained by flush mounting one microphone at the cavity base and the other flush with the side walls containing the orifice as shown in Figure 12. It is important to locate the incident microphone sufficiently far from the specimen to avoid near field effects. The microphone should be located sufficiently close, however, so that the separation distance is small relative to the incident sound wavelength. This is necessary to insure accurate measurements of the incident sound wave amplitude and phase. A discussion of the errors associated with using the two-microphone method is contained in Appendix A.

A schematic of the instrumentation used to conduct the experiments is shown in Figure 13. To generate incident sound pressure levels up to 150 dB, a JBL type 2480 driver capable of producing in excess of 10 watts of relatively "clean" acoustic power is used as the sound source. The .0508 meter diameter driver throat is coupled to the test section by means of a .0508 meter to .1016 meters diameter exponential expansion, JBL type H-93. Sound pressure levels in excess of 150 dB exceed the input capability of the GR-1560-P42 preamp. A 10 dB microphone attenuator, GR Type 1962-3200 has been added, which extends the

measurement range accordingly.

The signal generated by the Heath 1G-18 audio generator is amplified by the McIntosh MC2100 100 watt/channel power amplifier to power the JBL driver. The audio generator provides a tracking signal for the AD-YU Synchronous Filter and phase meter system. The 1036 system filters the two microphone input signals to the tracking signal frequency with a bandwidth of 5 Hz. The AD-YU Type 524A4 Phase Meter reads phase angle between the signals independent of signal amplitudes. The phase angle output is displayed on the AD-YU Type 2001 digital volt meter. A General Radio-1565 1/10 octave filter together with a Heath Type 1M2202 DVM is used to record the output signals from each of the two microphones. Also the two signals are observed on a TEK 533 Oscilloscope to visually note approximate phase and distortion effects.

The output of the incident microphone channel of the synchronous filter is used as a control voltage for an automatic level control amplifier. This control amplifier adjusts the drive level to the power amplifier in such a way as to keep the incident level constant, independent of frequency and amplitude response irregularities in the loudspeaker and tunnel.

As a convenience, a triple ganged 5 dB per step ladder attenuator is used to simultaneously increase the power amplifier drive level and decrease the synchronous filter input signals so that the control loop of the automatic level control amplifier always has the same gain. This has the added advantage keeping the levels at the AD-YU Filter input constant for all testing levels. Since the AD-YU Filter displays a small amplitude-phase dependency, this automatic level control improves accuracy as well as speed of data acquisition. A phase tracking test of both microphones mounted flush in the wind tunnel wall indicated accurate phase tracking within $\pm 0.2^\circ$ over a sound pressure level range of 70-150 dB.

4.2 Test Results

Figures (14)-(16) summarize the effects of grazing flow and sound pressure level on the acoustic resistance of specimens #1-10. *Grazing flow is shown to increase only negligibly the zero grazing flow resistance data.* Only grazing flow data corresponding to incident sound pressure levels greater than 110-120 dB are presented to insure an adequate signal-to-noise ratio. In agreement with the steady-state flow resistance data, the zero grazing flow data show that nonlinearity effects are important only for the Fibermetal FM 134 porous material - specimens #1, 5, 6 and 7. Nonlinearity effects are unimportant for specimens #2, 3, 4, 8, 9 and 10.

The effects of grazing flow and sound pressure level on the acoustic reactance of specimens #1-10 are summarized in Figures (17)-(25). In all cases, the porous face-sheet reactance and total system reactance (i.e., face-sheet and cavity reactance) are either unaffected or changed by only small (but measurable-like 10% differences) amounts from their zero grazing flow, low sound pressure level values. The frequency at which the reactance measurements were conducted requires special comment. For each specimen tested, the frequency of the incident sound field was selected so that at zero grazing flow and at an incident sound pressure level of 90 dB, the phase shift across the specimen face-sheet was ninety degrees. Under these conditions, the total reactance of each specimen was zero corresponding to resonance.

Figures (26)-(31) summarize the acoustic response of specimens #1, 2 and 7 to variations of frequency. In general, measurements show that the acoustic resistance is independent of frequency as shown, for example, in Figure 26. Specimens #2 and 7 show, however, an interesting dip in resistance in the neighborhood of 700-750 Hz. The dip occurs regardless of the amplitude of the incident sound or the speed of the grazing flow. Impact measurements showed that mechanical resonance corresponding to the first resonant clamped mode occurred at 1550 Hz for specimen #1, 730 Hz for specimen #2, and 360 Hz for specimen #7. This accounts for the observed resistance dips for specimens #2 and 7 - it corresponds to the excitation of the simple-harmonic fundamental mechanical resonance of the porous face-sheet material of specimen #2 and possibly to a higher harmonic of specimen #7. The dip in resistance physically corresponds to the sound particle field converting less mechanical energy into heat within the porous material.

The corresponding variation with frequency of the face-sheet and total reactance of specimens #1, 2 and 7 are shown in Figures (29) thru (31). Figure 29 shows that both the face-sheet and total reactance of specimen #1 to increase almost linearly with frequency. Figures 30 and 31, however, show the face-sheet reactance of specimens #2 and 7 to increase abruptly at the frequency corresponding to mechanical resonance. The total reactance of these specimens were only slightly perturbed at mechanical resonance. This is more clearly shown in Figure 32 which shows the sound pressure amplitude ratio across the specimen to increase significantly for specimen #2 with virtually no increases for specimen #1 and 7. Figure 32 also shows that specimen #2 experiences a large phase change between 700-750 Hz; however, specimens #1 and 7 do not.

To support the nongrazing flow two-microphone test results, the impedance of the ten porous samples were measured in a 1.83 meter long, .0508 meter diameter impedance tube. Since the

impedance method is well known it will not be described herein. The impedance tube test data are compared with the nongrazing flow d.c. resistance and two-microphone impedance test data in Table V. *Here the two-microphone data are corrected for acoustic radiation from the specimens using the method described in Appendix A.* Comparison of the d.c. and a.c. resistance is generally quite good. To first order, d.c. and a.c. resistances are equal. Comparison of the reactance data between the two-microphone and impedance tube measurement methods is only fair. It is extremely difficult to measure accurately using an impedance tube the reactance of a specimen whose resistance is close to ρc . Thus the two-microphone method of measuring reactance is believed to be superior to the impedance tube method.

4.3 Derivation of Non-Grazing Flow Impedance Prediction Model

A prediction model is derived of the impedance of thin porous-faced cavity-backed liners. Since the liner thickness is very small compared to the sound wavelength, the model will be derived using the concepts of lumped elements (i.e., the slug-mass model). This method was used by Rayleigh¹⁹ in deriving the impedance of the Helmholtz resonator. Rayleigh's approach is non-fluid mechanical but gives the actual acoustic impedance characteristics for low sound pressure levels (i.e., the "linear" impedance regime) when an empirical end correction is added to the slug mass.

Rayleigh derived the following expression for the impedance of a single orifice of diameter d and thickness τ backed by a cavity of length L ,

$$Z \approx \underbrace{R_{a.c.}}_{\text{orifice resistance}} / P + i \left[\underbrace{\rho \omega (\tau + .85 d)}_{\text{orifice inertia reactance}} - \underbrace{\rho c \cot \left(\frac{\omega L}{c} \right)}_{\text{cavity stiffness reactance}} \right] / P \quad (44)$$

where P is defined as the ratio of orifice area to cavity cross-sectional area. The impedance defined by Eq. (44) has been referenced to the cavity cross-sectional area. The impedance defined by Eq. (44) can be used to model the impedance of the porous materials by replacing the orifice a.c. resistance with the d.c. resistance of Eq. (41) with $\alpha=0.8$ and $\beta=1865$ (the data described in Section 4.2 showed this to be a good approximation) and by rewriting $d=\sqrt{P}D$ (for the cylindrical cavity shown in Figure 12, $P=(d/D)^2$) leads to the following estimate,

$$Z_{\text{porous}} \approx 1865 \left(\frac{\mu}{\delta} \right) \left(\frac{1-P}{P} \right) (1.8-P) + i \left[\rho \omega (\tau + \epsilon \sqrt{P} D) - \rho c \cot \left(\frac{\omega L}{c} \right) \right] / P \quad (45)$$

Here the constant 0.85 in Eq. (44) is replaced with an unknown (hopefully) constant ϵ to be determined from experimental data. The various values of ϵ computed using Eq. (45) and the two-microphone measured values of face-sheet reactance are summarized in Table VI. With the exception of specimens #5, 6 and 7, ϵ is seen to be constant with average value $\epsilon_{AV} \approx 0.52$ independent of specimen properties for both the Feltmetal and Rigimesh specimens. The lack of agreement between specimens #5, 6 and 7 and the remaining specimens cannot be explained. The excellent agreement among the remaining specimens is encouraging and suggests that specimens #5, 6 and 7 (which should be equivalent to specimen #1) may be improperly fabricated by the manufacturer.

The final expression for the face-sheet reactance, valid for all ten specimens, is

$$\left(\frac{X_f}{\rho \omega D} \right) \approx \left(\tau_D + 0.52 \sqrt{P} \right) / P \quad (46)$$

The substitution for the Feltmetal specimens of the d.c. for the a.c. resistance is valid only for low frequencies. A physical explanation for the low frequency restriction is described below.

The steady state model described in Section 3.3 will now be extended to unsteady flows. What is required is a reasonable estimate of the fluctuating drag of a cylinder immersed in a sound pressure field. It is assumed that most of the forces exerted by an oscillating sound field on a cylinder occur in the form of fluctuating wall shear stresses τ_w . Thus, the drag force per unit cylinder length is balanced by a shear force per unit cylinder length given by

$$D' = \tau_w' \delta \sim \mu \left(\frac{\partial v_x'}{\partial y} \right)_w \delta \sim \frac{\mu v_x' \delta}{L_{ch}} \quad (47)$$

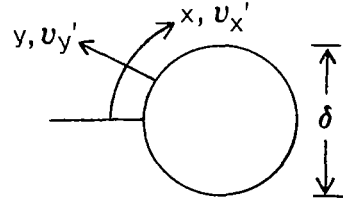
Here μ is the fluid coefficient of viscosity, δ is the cylinder diameter, L_{ch} is the extent to which the unsteady shear stresses diffuse laterally from the cylinder surface and v_x' is the amplitude of the fluctuating sound particle velocity.

An order-of-magnitude estimate of the high frequency solution to Eq. (47) is described below. The estimate starts with the boundary-layer approximations to the momentum equation for an unsteady flow past a stationary cylinder,

$$\frac{\partial v_x'}{\partial t} + v_x' \frac{\partial v_x'}{\partial x} + v_y' \frac{\partial v_x'}{\partial y} = -\frac{1}{\rho} \frac{\partial p'}{\partial x} + \nu \left(\frac{\partial^2 v_x'}{\partial y^2} \right) \quad (48)$$

The boundary-layer assumptions require that the lateral region of unsteady diffusion of vorticity be small w.r.t the cylinder radius. Physically this requires high frequency sound oscillations. Linearizing Eq. (48), and solving for the pressure gradient yields

$$\frac{\partial p'}{\partial x} = -\rho \frac{\partial v_x'}{\partial t} + \mu \frac{\partial^2 v_x'}{\partial y^2} \quad (49)$$



Far from the surface of the cylinder (see sketch), that is for sufficiently large values of y , the particle velocity must satisfy the following boundary conditions,

$$\lim_{y \rightarrow \infty} \frac{\partial v_x'}{\partial y} = 0 \quad \text{and} \quad v_x' = v'e^{i\omega t} \quad (50)$$

where v' is the amplitude of the sound particle velocity field. The corresponding sound pressure field becomes,

$$\frac{\partial p'}{\partial x} = -\rho \frac{\partial}{\partial t} (v'e^{i\omega t}) \quad (51)$$

Since the pressure is transmitted through the boundary-layer without change (this is one of the major benefits of boundary-layer theory), Eq. (49) may be rewritten as

$$\frac{\partial v_x'}{\partial t} = \frac{\partial}{\partial t} (v'e^{i\omega t}) + \nu \frac{\partial^2 v_x'}{\partial y^2} \quad (52)$$

The solution to Eq. (52) that satisfied the boundary condition given by Eq. (50) and the no-slip wall boundary conditions, $v_x' = 0$ at $y=0$, is

$$v'_x(y, t) = v'e^{i\omega t} \left[i - e^{-(1+i)\sqrt{\frac{\omega}{2\nu}} y} \right] \quad (53)$$

An estimate of the fluctuating drag D' follows from Eq. (53) upon substitution into Eq. (47) to yield

$$D' \sim \mu \left(\frac{\partial v'_x}{\partial y} \right)_{y=0} \delta = (1+i) \mu \delta \sqrt{\frac{\omega}{2\nu}} v'e^{i\omega t} \quad (54)$$

Comparing Eq. (54) and (47), the characteristic thickness L_{ch} of the fluctuating shear stress is

$$L_{ch} \sim \sqrt{\nu/\omega} \quad (55)$$

For Eq. (55) to be valid, the characteristic length $L_{ch} \ll \delta$, the cylinder diameter. This restricts the frequency f to the following regime,

$$f \gg \frac{\nu}{2\pi\delta^2} \quad (56)$$

Substituting the maximum values of $\delta=10^{-4}$ meter (Specimens #1, 5, 6, 7) from Table IV into Eq. (56), f must exceed the minimum value (for the ten specimens) of $f \gg 240$ Hz. Since the frequencies at which specimens #1, 5, 6 and 7 were tested never exceeded $f=1200$ Hz, the effects of frequency should be small in accord with the measurements shown in Figure 26. Thus in light of the above analysis, the agreement between a.c. and d.c. resistances is to be expected. At very high frequencies, however, the a.c. resistance should become much larger than the d.c. resistance.

5. CONCLUSIONS

The results of this study have immediate application to the control of internally generated noise within jet engines. Steady-state and acoustic tests were performed on seven Feltmetal and three Rigimesh porous lining materials. The principal findings of this study are summarized in terms of the material steady-state and acoustical behavior.

5.1 Steady-State Flow Resistance

(1) The effects of grazing flow on the resistance of thin porous-faced liners were measured and found to be generally small except for specimen #7.

(2) The data for the seven Feltmetal specimens were correlated in terms of a semi-empirical fluid mechanical model that treated the porous material as a collection of interacting small cylinders. The correlation, shown below, is not general but does indicate the qualitative behavior of the resistance in terms of the material and medium (air) properties.

$$R_{d.c.} \simeq 1865 \left(\frac{\mu}{\delta} \right) \left(\frac{1-P}{P} \right) (1.8 - P)$$

(3) The nonlinear behavior of the specimens was correlated in terms of a fiber diameter based Reynolds number $Re = V_D \delta / \nu$. In general, the onset of nonlinearity occurred when Re ranges from 2 to 3. Both the data and the correlation indicate that small diameter fibers delay nonlinearity to higher specimen through flow speeds.

5.2 Acoustic Impedance

(1) The effects of grazing flow on the resistance and reactance of thin porous-faced liners were measured and found to be generally small.

(2) A simple lumped element model was derived which correlated the face-sheet reactance of the ten specimens. The correlation, shown below, was derived by treating the porous material as an equivalent orifice of area PA where A is the cavity backing area and P is the material porosity,

$$X_f \simeq \rho \omega \left(\tau - 0.52 \sqrt{P} D \right) / P$$

A simple prediction expression for the impedance of the seven Feltmetal specimens was derived based on the substitution for sufficiently low frequencies of the a.c. resistance by the d.c. resistance. An analysis presented in Section 4.3 showed that the a.c. and d.c. resistances are approximately equivalent for frequencies $f \ll \nu / 2\pi \delta^2$ where ν is the kinematic viscosity of the fluid and δ is the mean diameter of the Feltmetal material. The resulting expression is

$$Z \approx 1865 \left(\frac{\mu}{\delta} \right) \left(\frac{1-P}{P} \right) (1.8-P) + i \left[\rho \omega (\tau + 0.52 \sqrt{P} D) - \rho c \cot \left(\frac{\omega L}{c} \right) \right] / P$$

An important finding of this study is that a great deal can be learned about the acoustic properties of porous lining materials in a jet engine duct environment by the much simpler study of their nongrazing flow, steady-state flow resistance behavior.

REFERENCES

1. Hersh, A. S. and Walker, B., "The Acoustic Behavior of Helmholtz Resonators Exposed to High Speed Grazing Flows", AIAA Paper No. 76-536, AIAA 3rd AeroAcoustics Conference, July, 1976.
2. Feder, E. and Dean, L. W., "Analytical and Experimental Studies for Predicting Noise Attenuation in Acoustically Treated Ducts for Turbo Fan Engines", NASA CR-1373, 1969.
3. Dean, P. D., "An In Situ Method of Wall Acoustic Impedance Measurements in Duct Flow", Journal of Sound and Vibration, 1974, Vol. 34, 97-130.
4. Plumblee, H. E. Jr., Dean, P. D., Wynne, G. A., and Burrin, R. H., "Sound Propagation in and Radiation from Acoustically Lined Flow Ducts: A Comparison of Experiment and Theory", NASA CR-2306, Oct. 1973.
5. Darcy, H. "Les Fontaines Publiques de la Ville de Dijon" Dalmont, Paris, 1856.
6. Bear, J., "Dynamics of Fluids in Porous Media", American Elsevier Publishing Company, N.Y., N.Y., 1972.
7. Scheidegger, A. E. *The Physics of Flow Through Porous Media*, 2nd ed., University of Toronto Press, Toronto, 1969.
8. Irmay, S., "On the Theoretical Derivation of Darcy and Forcheimer Formulas", Trans. Amer. Geophys. Union. No. 4., V-39, 702-707 (1958).
9. Kozeny, J., "Uker Kapillare Leitung des Wassers in Boden", Sitzungober, Ahod. Wiss. Wien., V. 136, 271-306 (1927).
10. Rumer, R. R. and Drinkar, P. A., "Resistance to Laminar Flow through Porous Media", Proc. Amer. Soc. Civil Eng. No. HY5, V. 92, 155-164 (1966).
11. Rumer, R. R., *Resistance to Flow Through Porous Media in Flow Through Porous Media* (R. J. M. deWiest, Ed), Academic Press, New York, 1969.
12. Iberall, A. S., "Permeability of Glass Wool and Other Highly Porous Media", J. Res. Nat. Bus. Stand, V45, 398-406 (1950).
13. Lamb, H., *Hydrodynamics*, 6th Ed., Cambridge Univ. Press, London (1932).

14. Blick, E. F., "Capillary Orifice Model for High Speed Flow Through Porous Media I & EC", Process Design and Development, No. 1, V. 5, 90-94 (1966).
15. Cheavetau, G. and C. Thirriot, "Regimes d'e'coulement en milieu poreux et limite de la loi de Darcy", La Houille Blanche, No. 1, V. 22, 1-8 (1967).
16. Scott, R. A., 1946 Proceedings of the Physical Society 58, 165-183, "The Absorption of Sound in a Homogeneous Porous Medium", also 1946 Proceedings of the Physical Society 58, 358-368, "The Propagation of Sound Between Walls of Porous Material".
17. C. Zwikker and C. W. Kosten, Sound Absorbent Materials, Elsevier Publishing Company, Inc., New York, 1949.
18. Morse, R. W., "Acoustic Propagation in Granular Media", J. Acoust. Soc. Am. V. 24, No. 6, 696-700 (1952).
19. Rayleigh, Theory of Sound, The Macmillan Company, New York, Vol. II.
20. Morse, R. W. and Bolt, R. H., "Sound Waves in Rooms", Revs. Modern Phys. V. 16, N. 2, 69-150 (1944).
21. Beranek, L. L., "Acoustical Properties of Sound Absorbing Materials", J. Acoust. Soc. Am., V. 19, No. 4, 556-568 (1947).
22. Zorumski, W. E. and Parrott, T. L., "Nonlinear Acoustic Theory for Rigid Porous Materials", NASA TND-6196, June 1971.
23. "Fluid Meters", American Society of Mechanical Engineers, Part 1 - 4th Edition, New York, 1937.
24. Beavers, G. S. and Joseph, D. D., "Boundary Conditions at a Naturally Permeable Wall", J. Fluid Mech., V. 39, 197-207 (1967).
25. Taylor, G. I., "A Model for the Boundary Condition of a Porous Material, Part I", J. Fluid Mech., V. 49, Part 2, 319-326 (1971).

TABLE I. SUMMARY OF MANUFACTURERS PREDICTED ACOUSTIC PROPERTIES

Spec. #	Trade Name or Identifica- tion	(Nominal) Predicted Resistance (Rayls-mks)	NLF* 500/20	Average Thickness (meters)			Porosity	Average Pore Diameter (meters)	
<u>Feltmetal Materials</u>									
1	FM 134	320@0.2m/sec	4.7	8.9x10 ⁻⁴			0.59	5.9x10 ⁻⁵	
2	347-10-20- AC3A-A	100	"	2.0	4.1	"	0.97	4.8	"
3	12581-4	580	"	NA**	9.1	"	0.80	3.2	"
4	FM-122	500	"	1.8	7.6	"	0.91	3.9	"
5	FM-134	320	"	4.7	8.9	"	0.59	5.9	"
6	FM-134	320	"	"	"	"	"	"	"
7	FM-134	320	"	"	"	"	"	"	"
<u>Rigimesh Materials</u>									
8	A0300S0204L	200@.6m/sec	NA	3.8	"		NA	1.8	"
9	A0300S0304L	300	"	NA	3.8	"	NA	"	"
10	A0300S0404L	400	"	NA	3.8	"	NA	"	"

* Material Nonlinear Factor defined as the ratio of flow resistances at flow velocities of 5.0 m/sec and 0.2 m/sec.

** Information not available

Table II. EMPIRICAL FIT OF D.C. FLOW RESISTANCE DATA
 $[R = a+bV_D \text{ (Rayls-mks)}]$

Specimen #	Blowing		Suction	
	$V_\infty=0$	$V_\infty=79.6 \text{ m/s}$	$V_\infty=0$	$V_\infty=79.6 \text{ m/s}$
1	$398+240V_D$	$394+250V_D$	$408+220V_D$	$419+210V_D$
2	$117+11V_D$	$120+126V_D$	$121+10V_D$	$113+10V_D$
3	$865+110V_D$	$860+120V_D$	$855+100V_D$	$847+90V_D$
4	$598+65V_D$	$581+67V_D$	$595+54V_D$	$567+61V_D$
5	$493+330V_D$	$489+330V_D$	$505+290V_D$	$563+250V_D$
6	$540+320V_D$	$538+320V_D$	$564+340V_D$	$570+330V_D$
7	$637+500V_D$	$644+500V_D$	$717+430V_D$	$733+420V_D$
8	$292+36V_D$	$297+37V_D$	$316+32V_D$	$298+29V_D$
9	$558+64V_D$	$524+76V_D$	$584+61V_D$	$572+48V_D$
10	$298+34V_D$	$296+35V_D$	$313+28V_D$	$282+29V_D$

TABLE III. SUMMARY OF CORRECTION TO ΔP_S MEASUREMENTS DUE TO GRAZING FLOW

Specimen #	Corrected ΔP_S (m-H ₂ O) at $V_D=0$	
	$V_\infty=56.39$ meters/sec (mks)	$V_\infty=79.55$ meters/sec (mks)
1	.0011 m-H ₂ O	.0023 m-H ₂ O
2	.0020	.0038
3	.0020	.0041
4	.0020	.0043
5	negligible	negligible
6	.0013	.0025
7	.0013	.0025
8	.0018	.0036
9	negligible	negligible
10	.0005	.0010

TABLE IV. CORRELATION OF D.C. FLOW RESISTANCE MEASUREMENTS

Spec. #	Rd.c (Rayls- mks)	Porosity (P)	Fiber Dia. (meters)	Corr. Para- meter* (β)	Obs. V_D at Onset of NL (meters/ sec)	Values of V_D where $Re=2;3$ (meters/ sec)
1	398	.51	10^{-4}	1784	.3-.4	.15;.23
2	117	.97	8×10^{-6}	2026	3-4	3.63;5.44
3	865	.80	8×10^{-6}	1538	.7-1.1	3;4.5
4	598	.92	4×10^{-6}	1737	2.5-3.8	6.92;10.4
5	493	.48	10^{-4}	1915	.35-.40	.15;.23
6	540	.46	10^{-4}	1907	.25-.35	.16;.24
7	637	.45	10^{-4}	2145	.15-.40	.16;.25
8	292	.37	4×10^{-5}	-	.7-2	.47;.71
9	558	.29	4×10^{-5}	-	1-1.5	.53;.80
10	298	.43	4×10^{-5}	-	.7-2	.43;.64

*The values of β tabulated above are determined from Eq. (41)
with $\alpha=0.8$

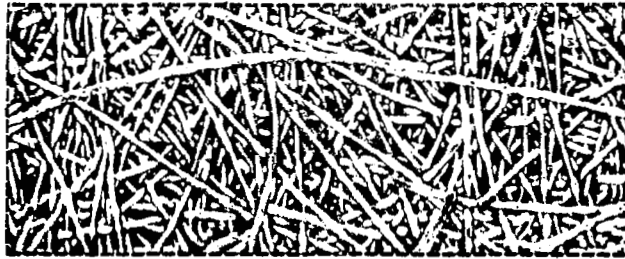
TABLE V. COMPARISON OF NON-GRAZING FLOW STEADY STATE, TWO MICROPHONE
AND STANDING WAVE TUBE MEASUREMENTS

Specimen #	Specific Resistance (Rayls-mks)			Face Sheet Reactance ($X_f/\rho\omega D$)	
	Steady Flow	Two-Mic*	Impedance Tube	Two-Mic*	Impedance Tube
1	400	405	395	.80	.72
2	115	141	130	.59	.28
3	890	931	906	.69	.40
4	600	684	710	.54	.77
5	500	515	548	1.14	.81
6	540	553	512	1.13	.79
7	650	676	687	1.32	.74
8	280	321	359	.79	1.16
9	560	585	528	.98	.90
10	280	235	285	.64	.68

*data corrected by method of Appendix A

TABLE VI. EXPERIMENTAL DETERMINATION OF INERTIAL CONSTANT ϵ

Specimen #	Thickness τ (m)	Porosity P	$\left[\frac{X_f}{\rho \omega D} \right]$ meas.	ϵ
1	9.6×10^{-4}	.51	.80	.55
2	9.6 "	.97	.59	.56
3	9.1 "	.80	.69	.59
4	7.8 "	.92	.54	.50
5	9.2 "	.48	1.14	.76
6	9.1 "	.46	1.13	.73
7	9.1 "	.45	1.32	.86
8	1.3 "	.37	.79	.48
9	1.1 "	.29	.98	.52
10	1.4 "	.43	.64	.43

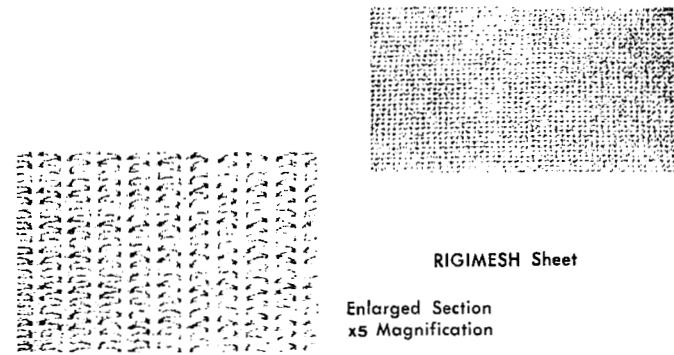


STAINLESS STEEL TYPE 430



Surface appearance at X 24 of 430 stainless steel FELTMETAL fiber metal. The material is 15% dense and employs Type B46 fibers.

Photographs of Feltmetal Porous Materials



Photograph of Rigimesh Porous Material

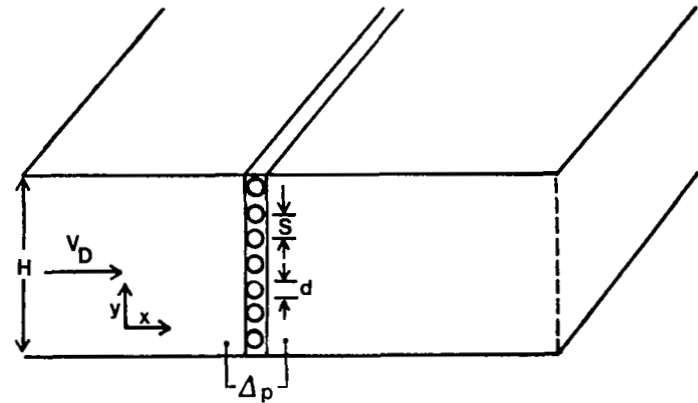


FIGURE 1. ENLARGED PHOTOGRAPHS OF SPECIMEN INTERIOR AND MODEL GEOMETRY

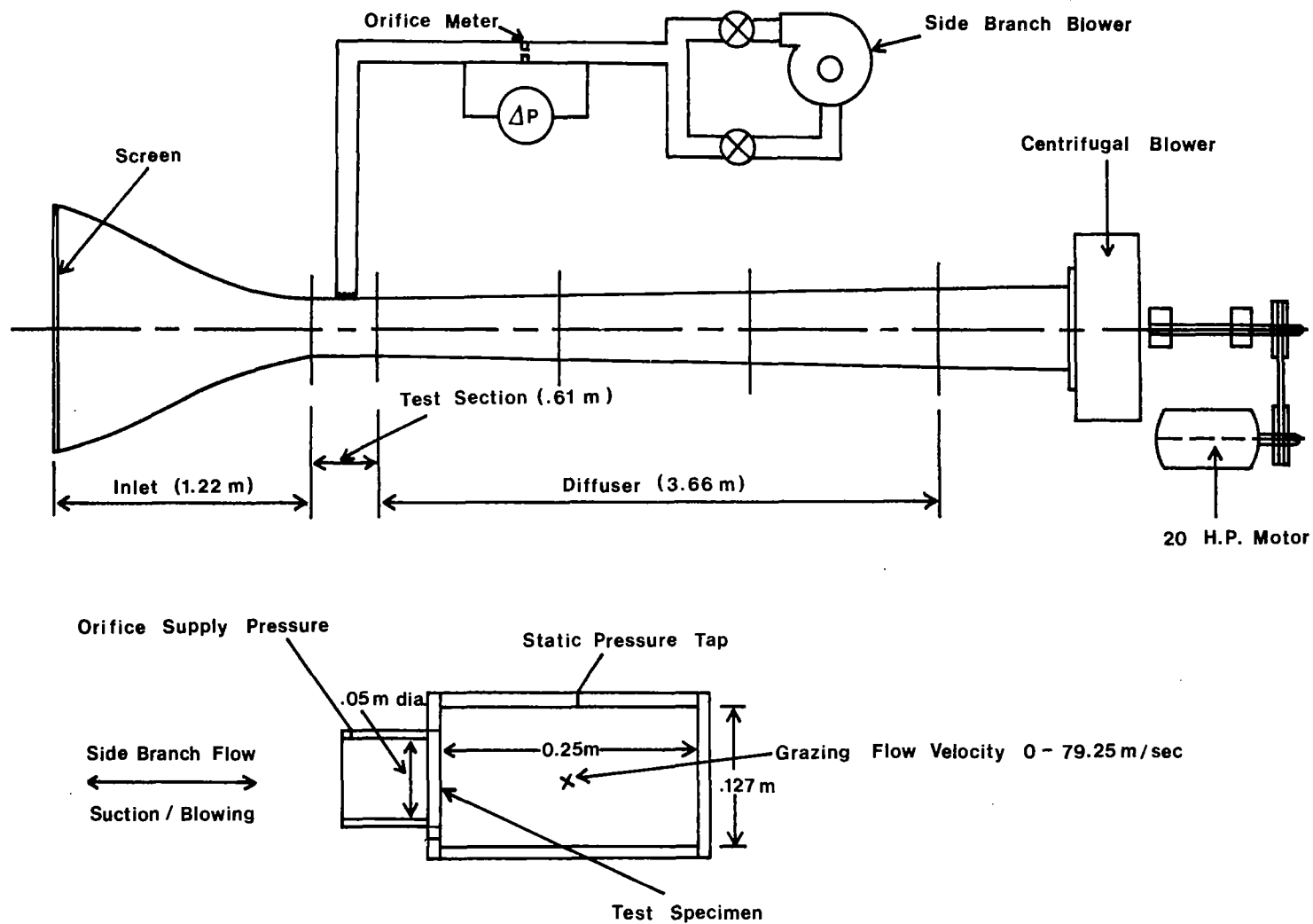


FIGURE 2. SCHEMATIC OF STEADY-STATE FLOW RESISTANCE MEASUREMENT SYSTEM

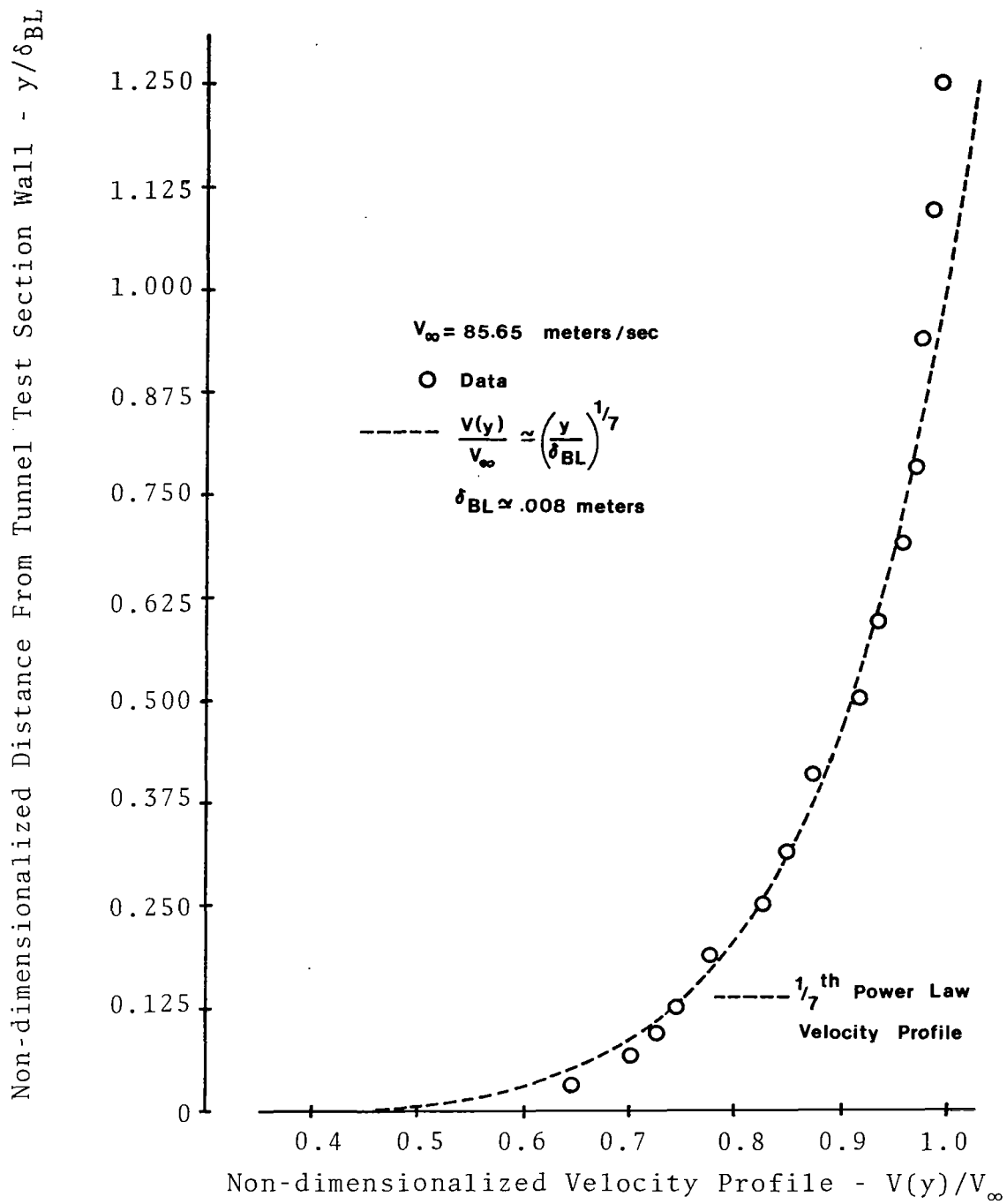


FIGURE 3. TEST SECTION BOUNDARY LAYER VELOCITY PROFILE

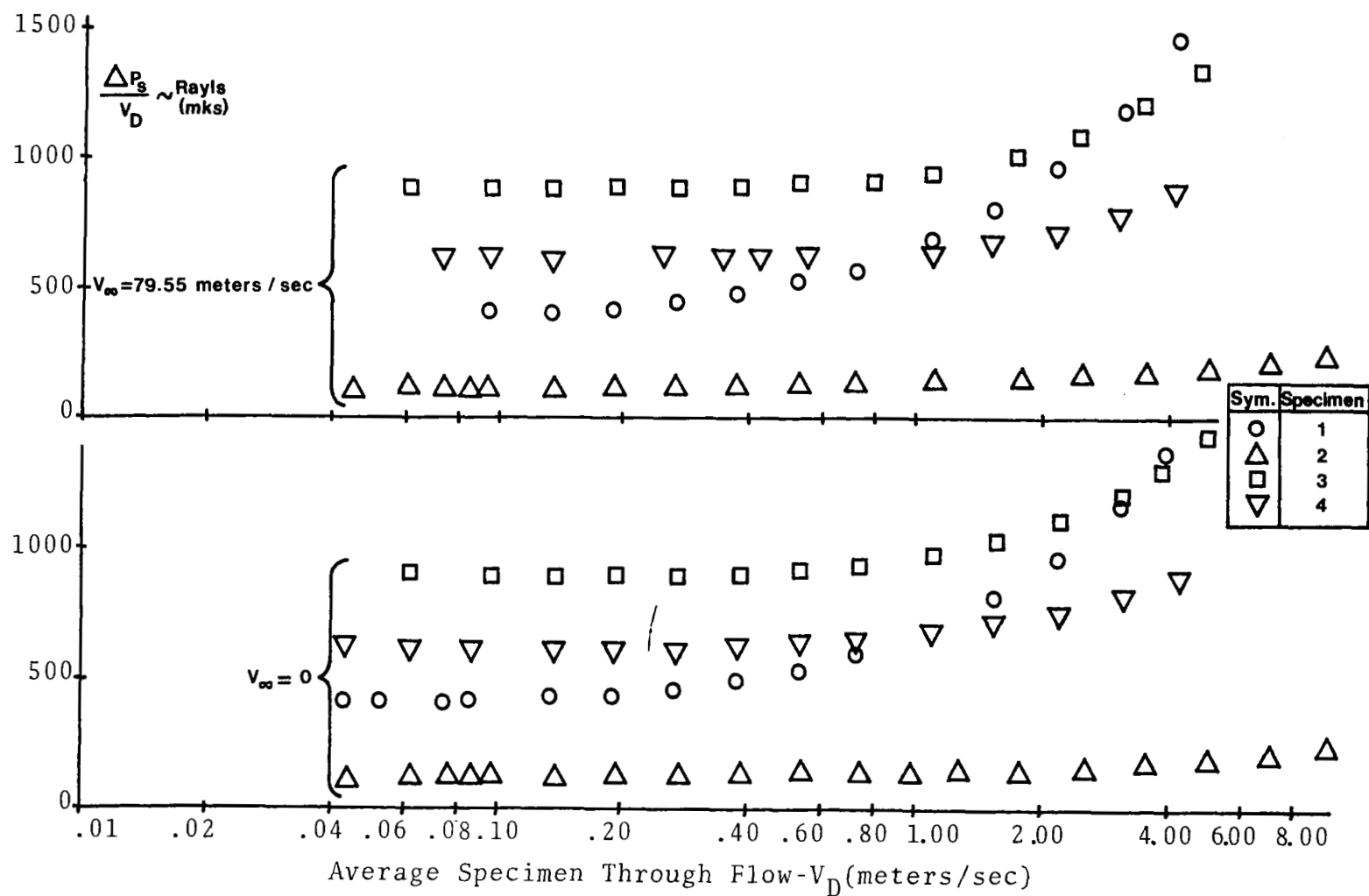


FIGURE 4. EFFECT OF GRAZING FLOW ON THE STEADY-STATE RESISTANCE OF SPECIMENS 1-4 OPERATING IN THE BLOWING MODE

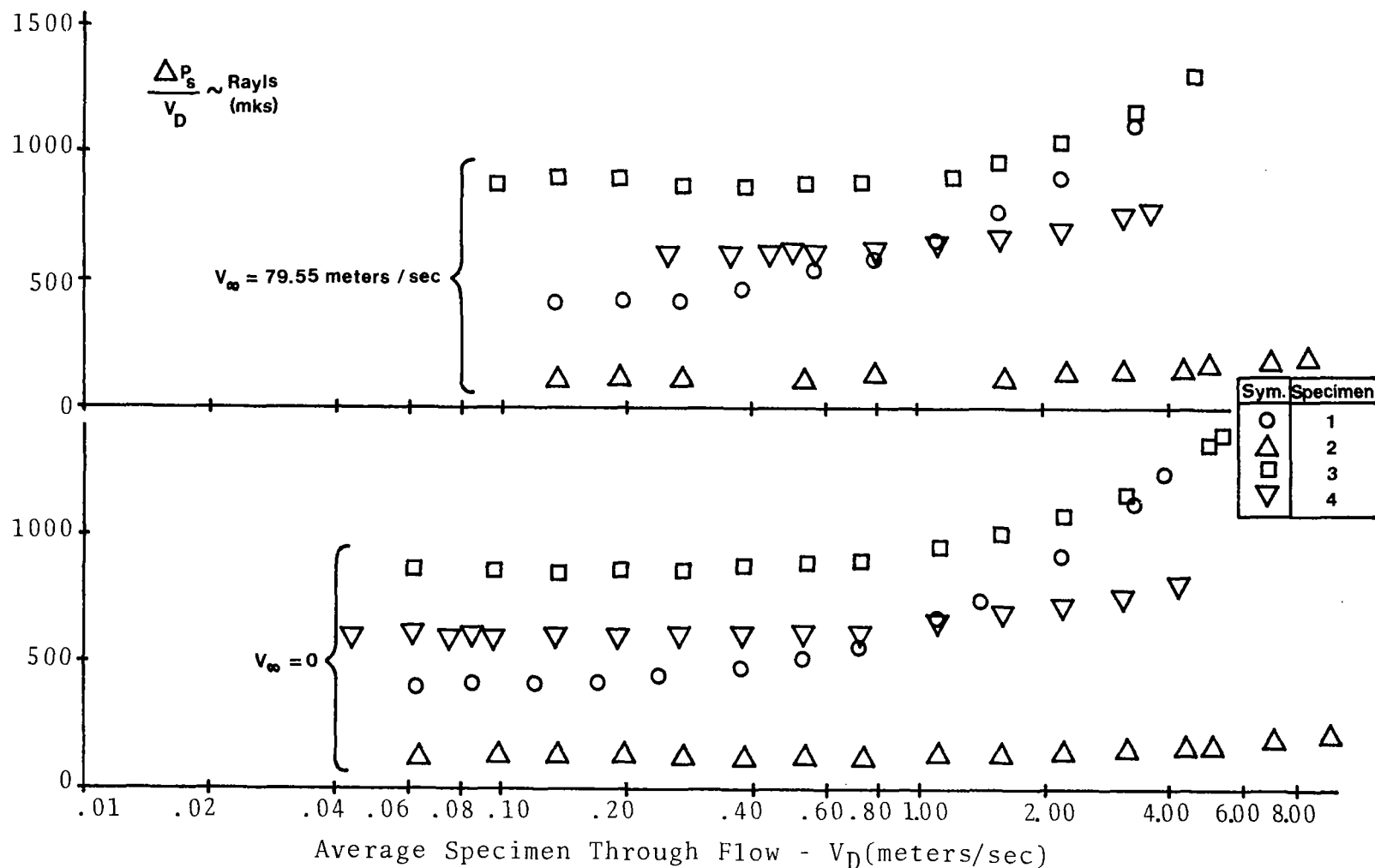


FIGURE 5. EFFECT OF GRAZING FLOW ON THE STEADY-STATE RESISTANCE OF SPECIMENS 1-4 OPERATING IN THE SUCTION MODE

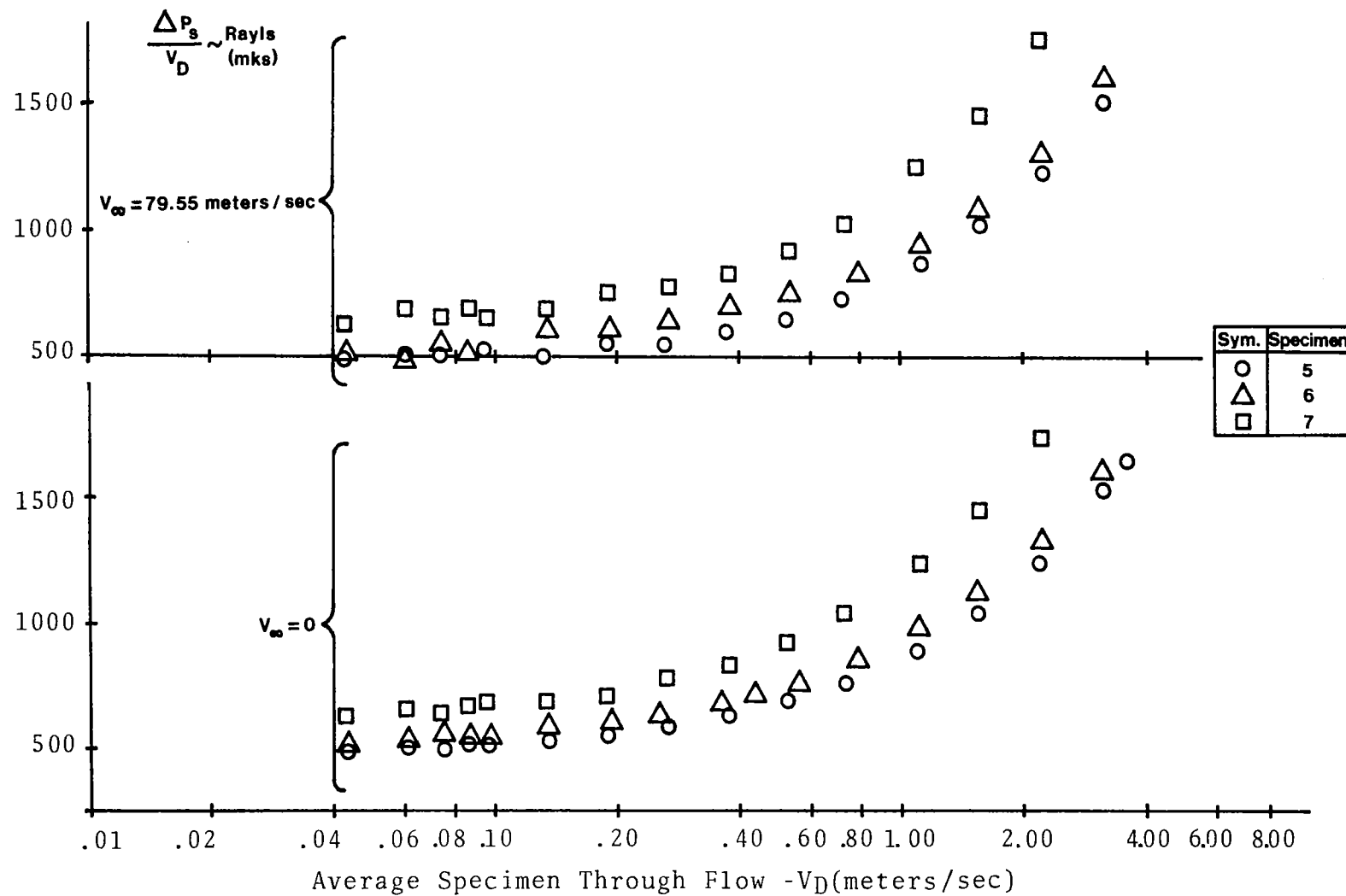


FIGURE 6. EFFECT OF GRAZING FLOW ON STEADY-STATE RESISTANCE OF SPECIMENS 5-7 OPERATING IN THE BLOWING MODE

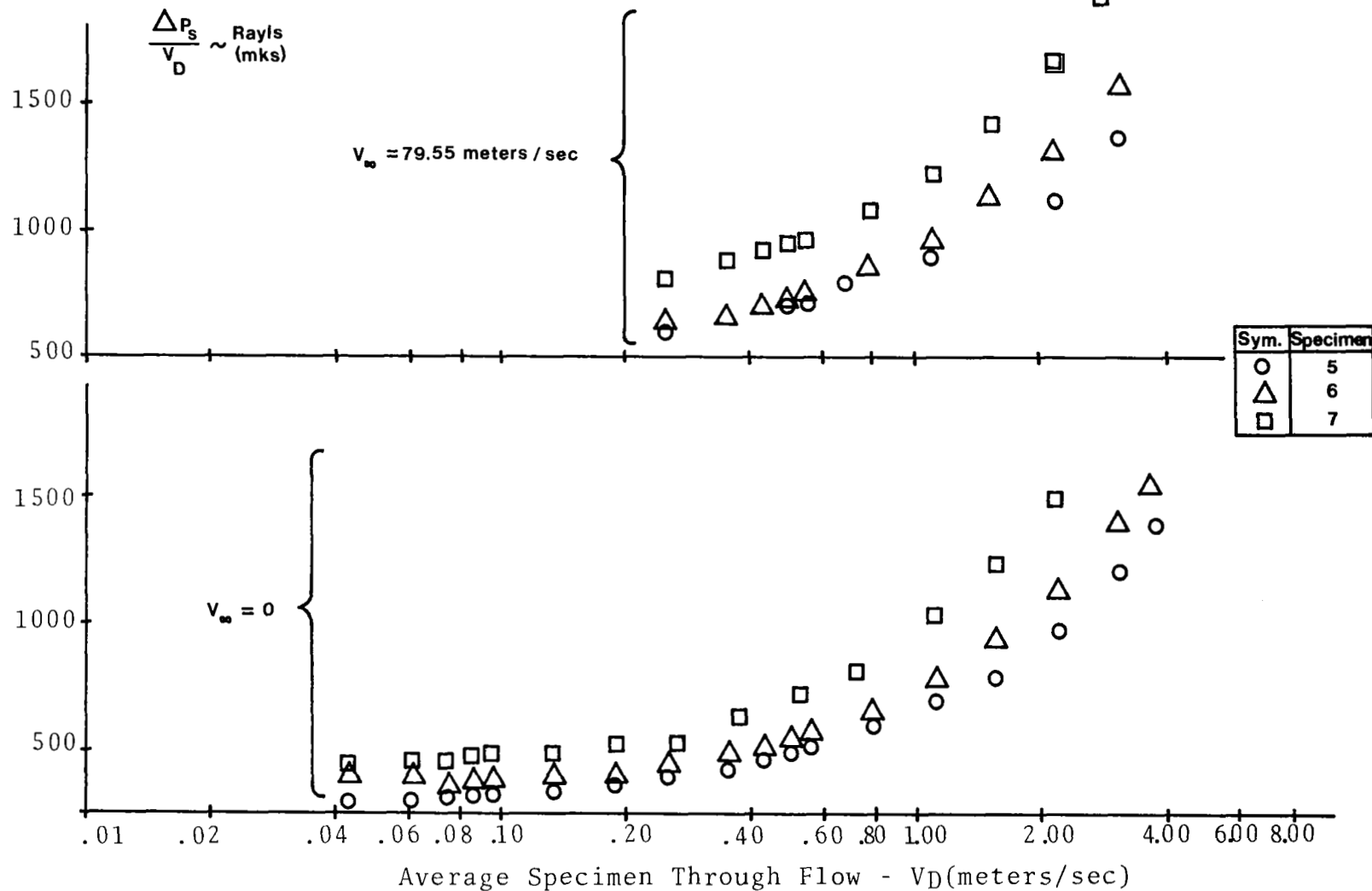


FIGURE 7. EFFECT OF GRAZING FLOW ON STEADY-STATE RESISTANCE OF SPECIMENS 5-7 OPERATING IN THE SUCTION MODE

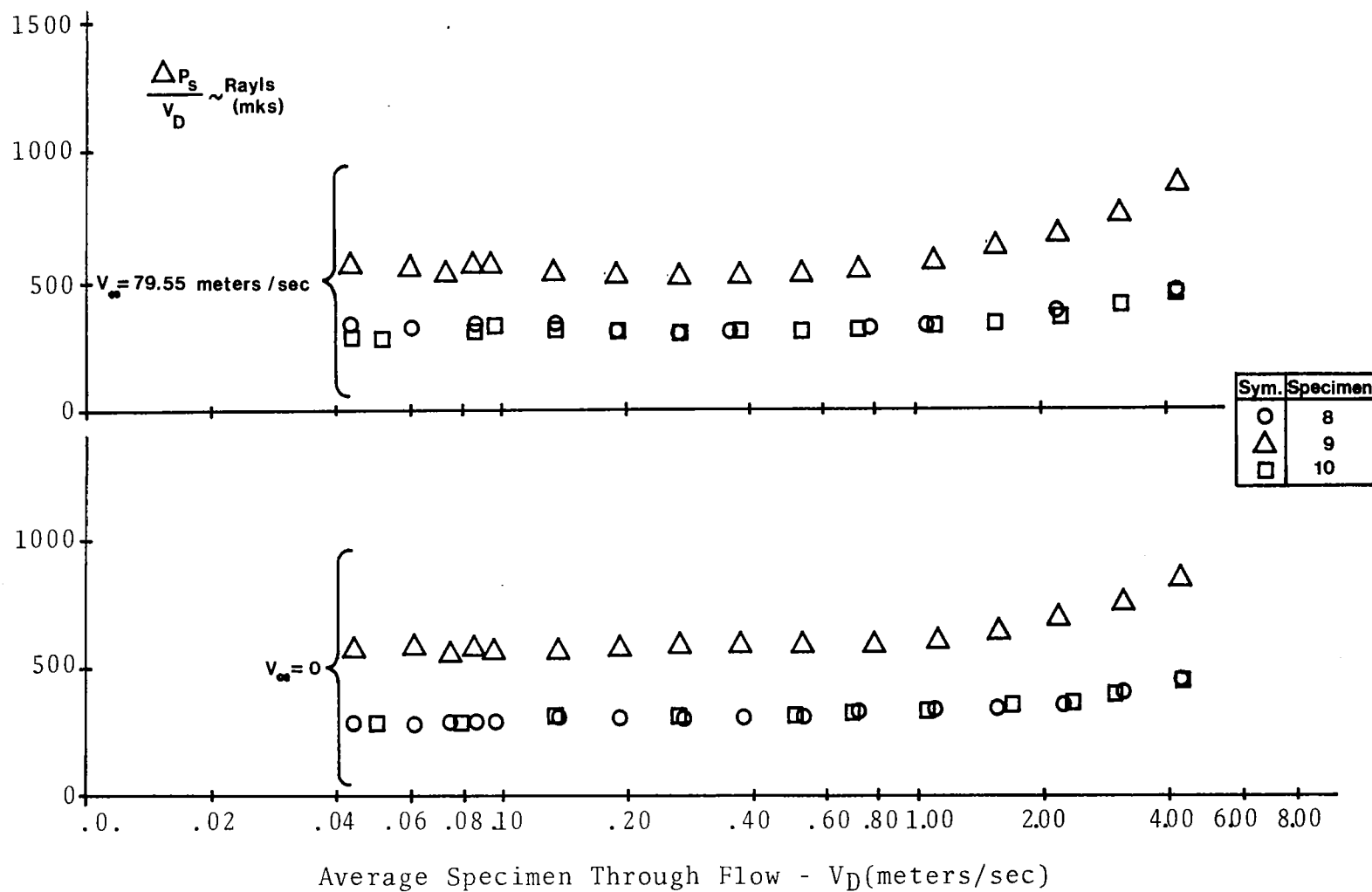


FIGURE 8. EFFECT OF GRAZING FLOW ON STEADY-STATE RESISTANCE OF SPECIMENS 8-10 OPERATING IN THE BLOWING MODE

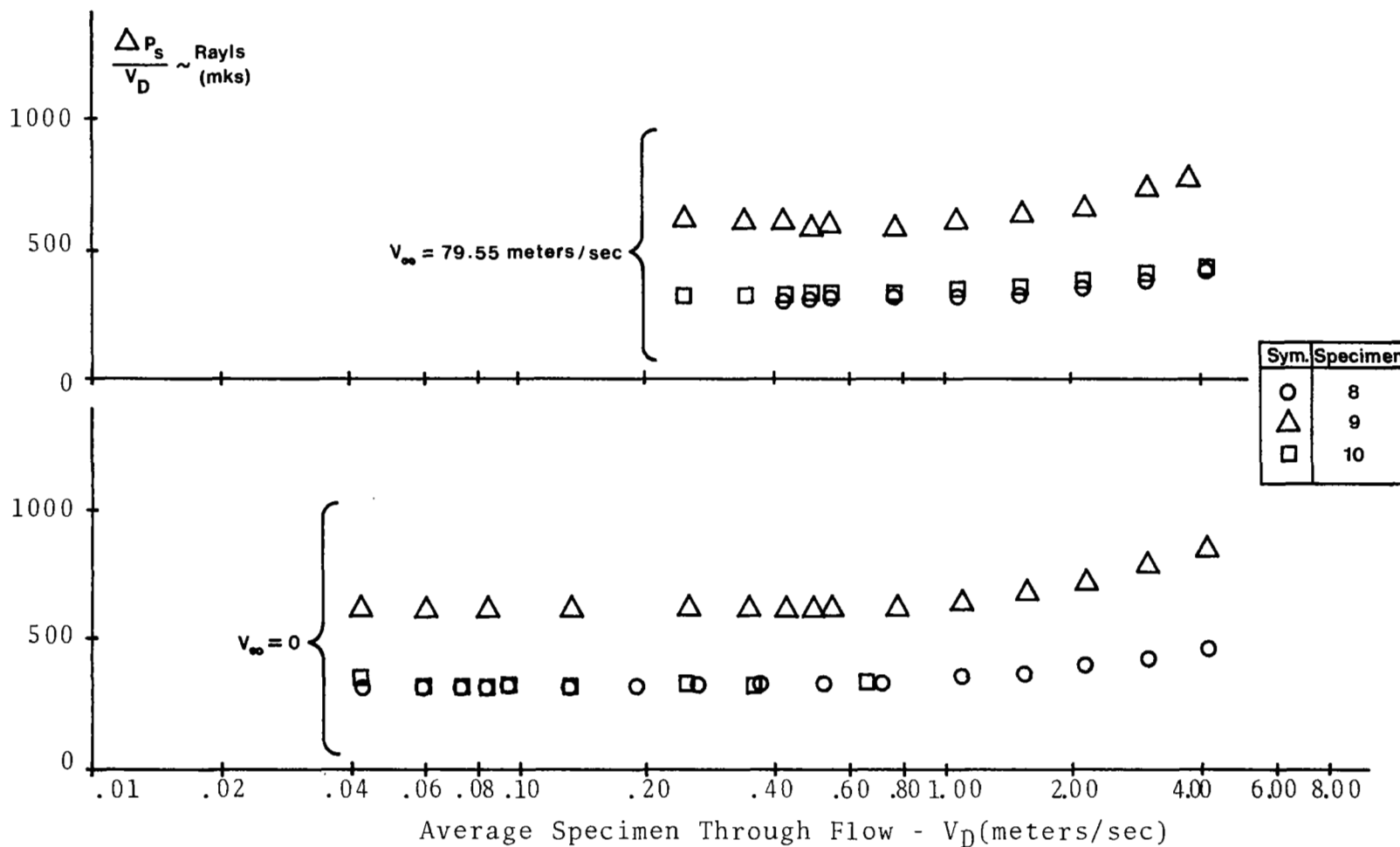


FIGURE 9. EFFECT OF GRAZING FLOW ON STEADY-STATE RESISTANCE OF SPECIMENS 8-10 OPERATING IN THE SUCTION MODE

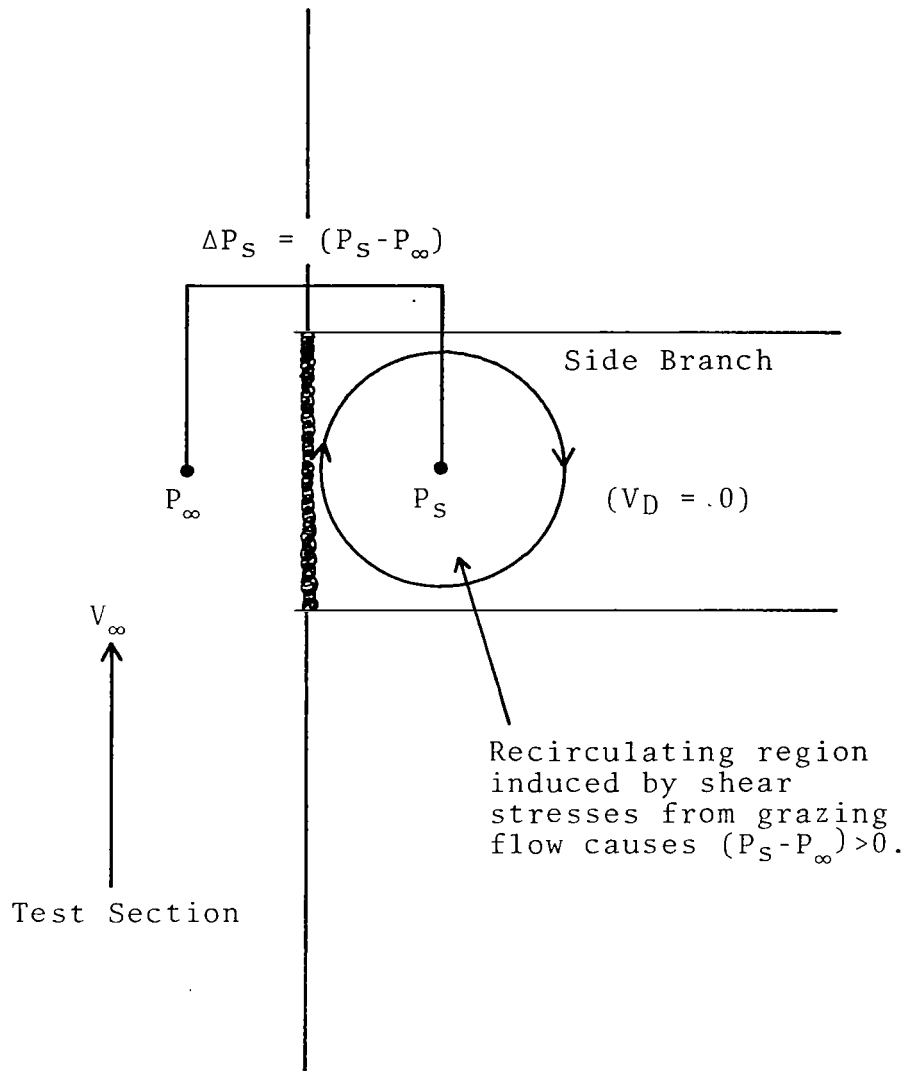


FIGURE 10. SCHEMATIC OF VORTICAL VELOCITY INDUCED ACROSS SPECIMEN BY GRAZING FLOW SHEAR STRESSES

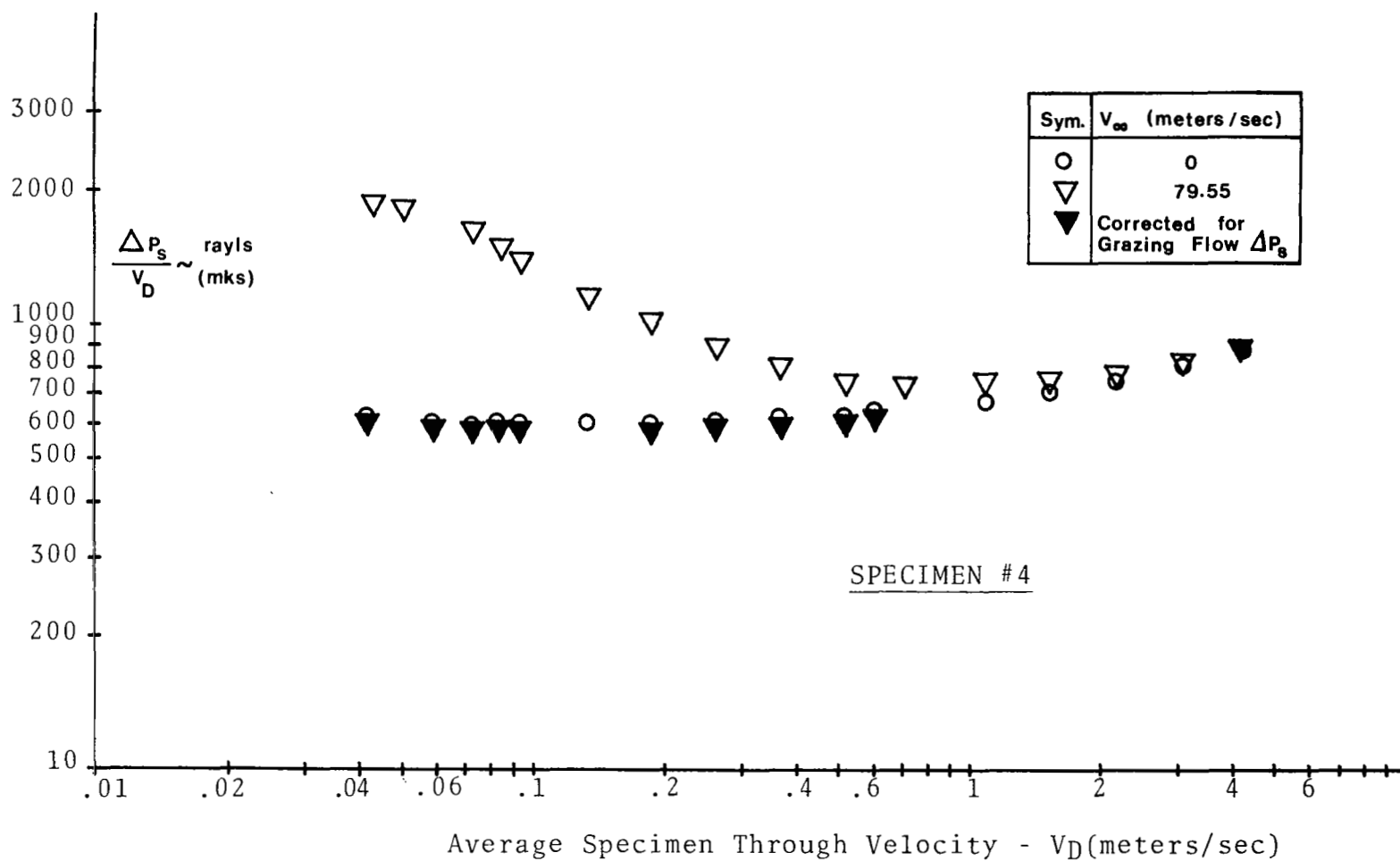


FIGURE 11. EFFECT OF GRAZING FLOW ON STEADY-STATE RESISTANCE OF SPECIMEN-BLOWING

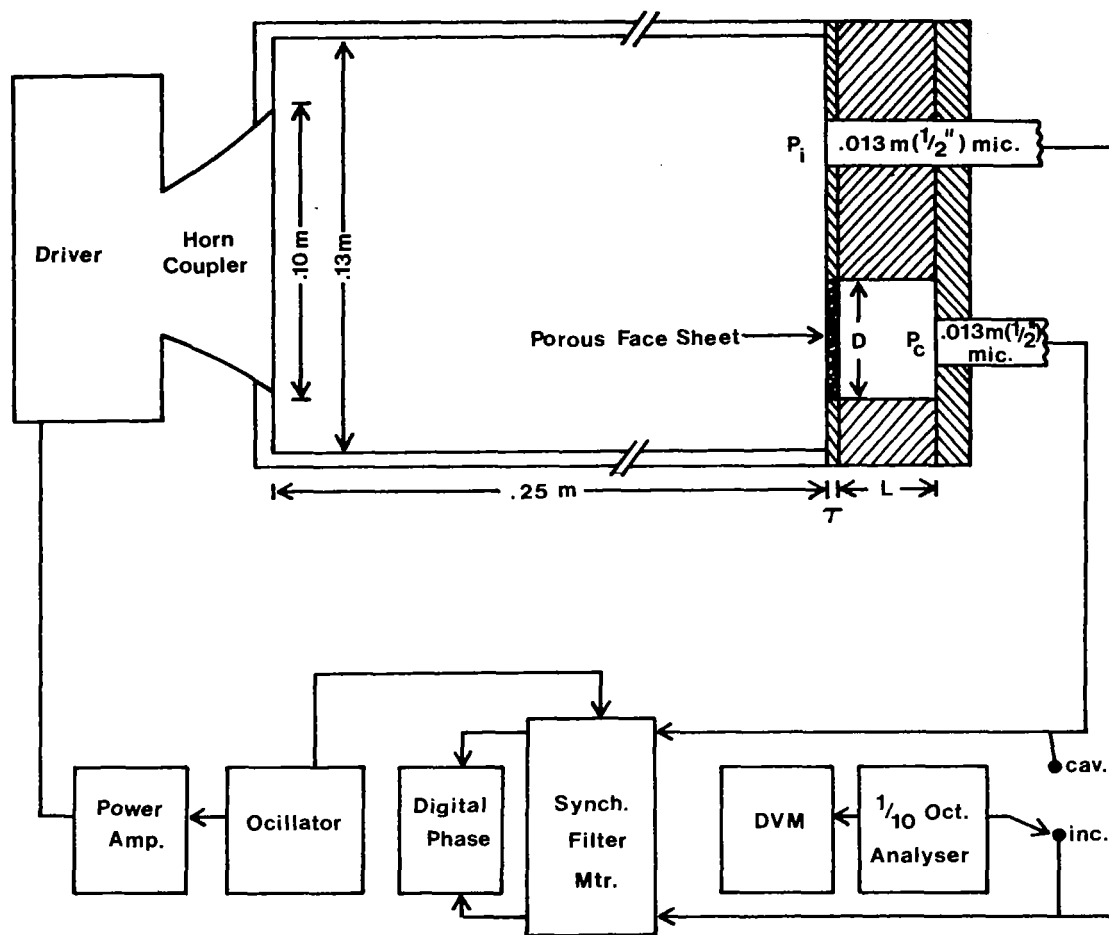


FIGURE 12. SCHEMATIC OF TWO-MICROPHONE MEASUREMENT SYSTEM

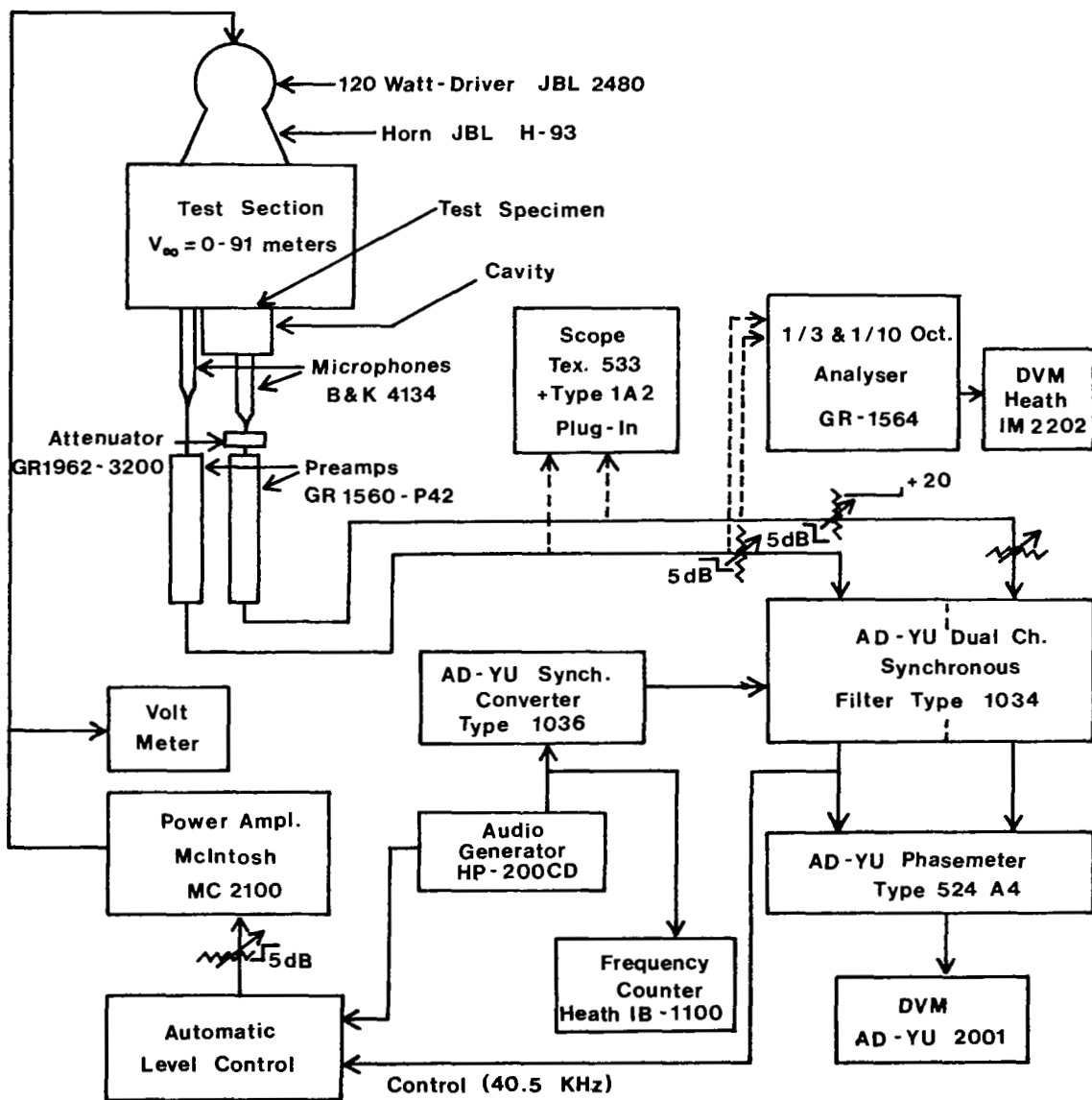


FIGURE 13. TWO-MICROPHONE METHOD INSTRUMENTATION

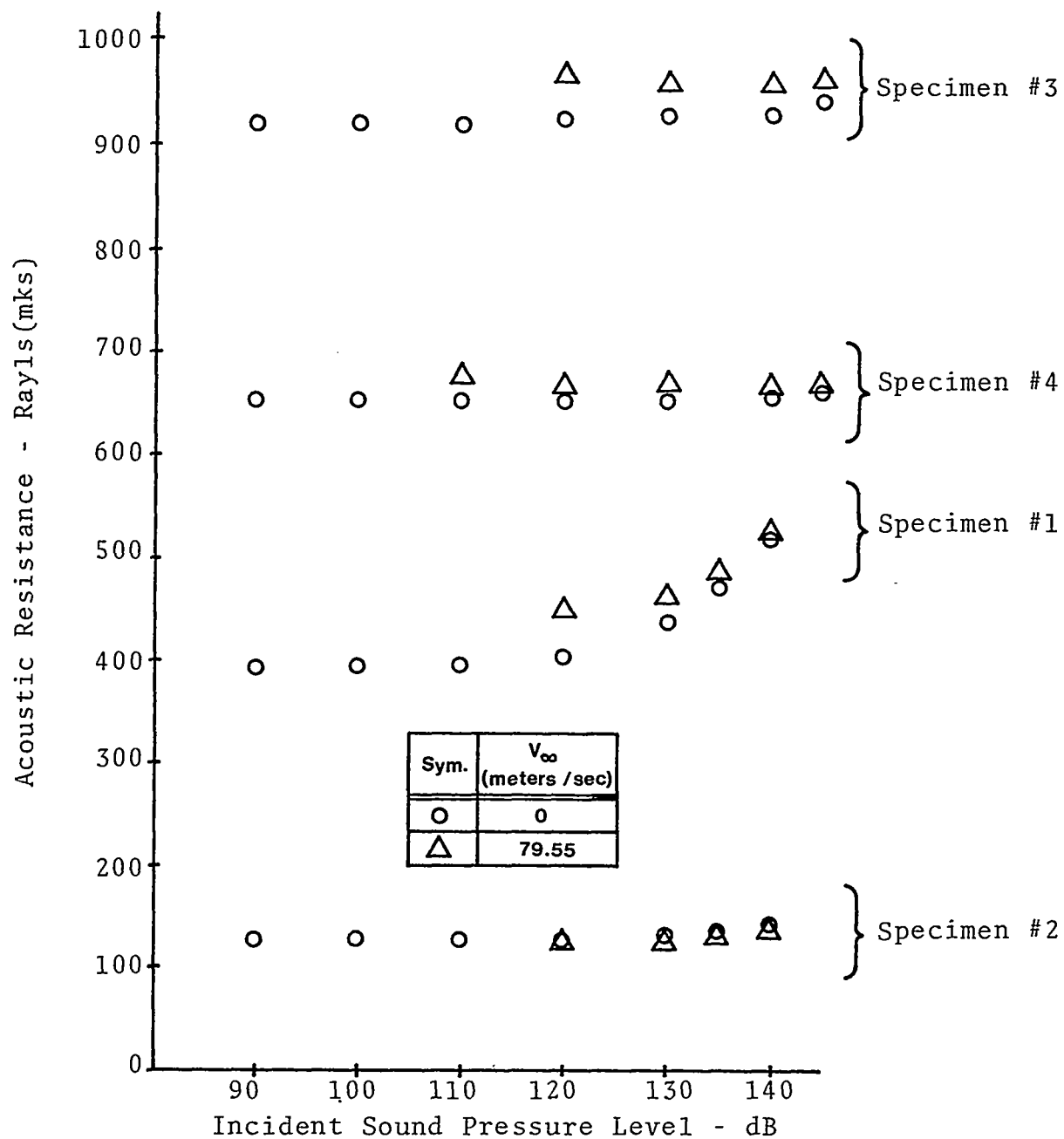


FIGURE 14. EFFECTS OF GRAZING FLOW AND SOUND PRESSURE LEVEL ON THE ACOUSTIC RESISTANCE OF SPECIMENS #1-4

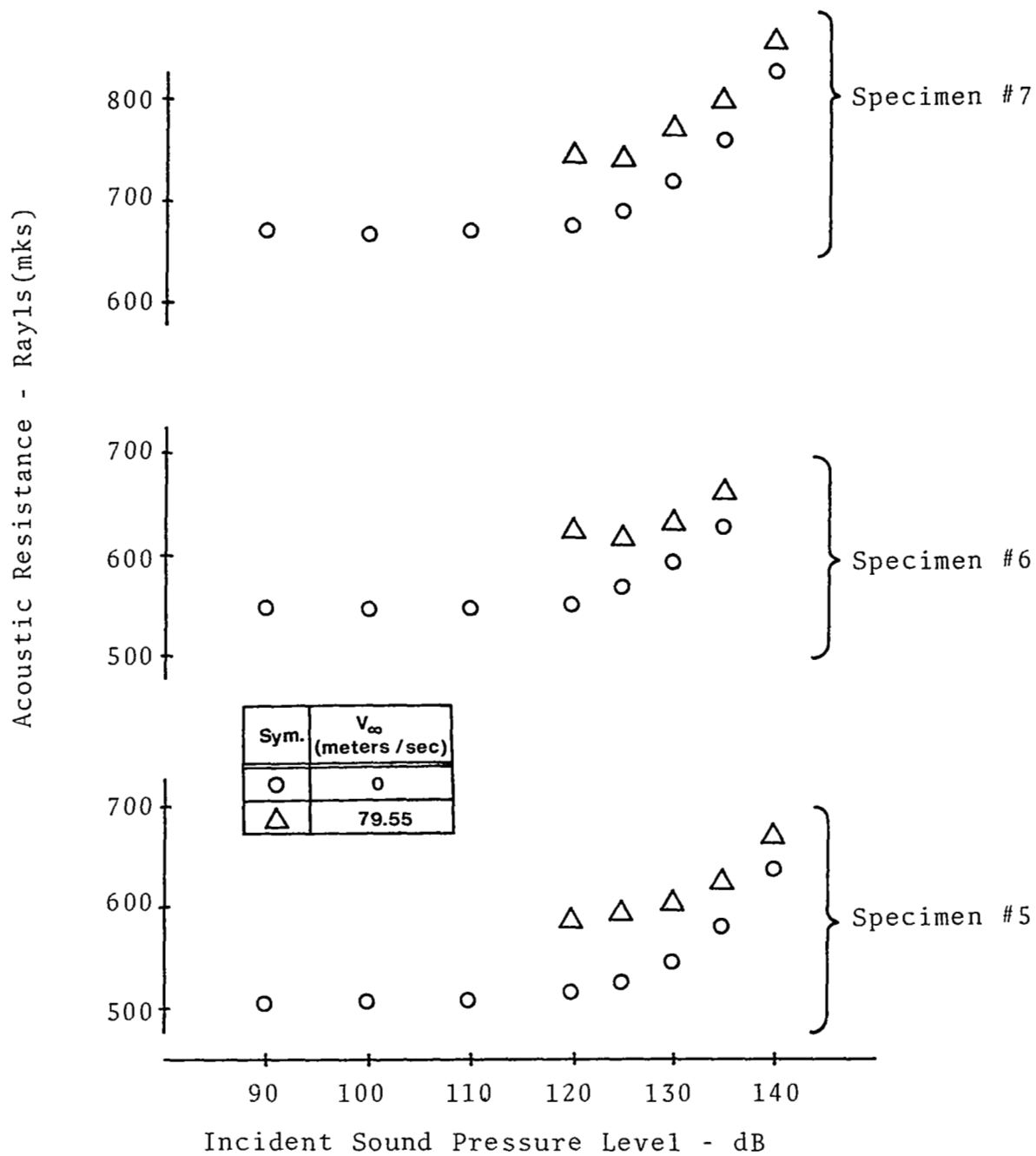


FIGURE 15. EFFECTS OF GRAZING FLOW AND SOUND PRESSURE LEVEL ON THE ACOUSTIC RESISTANCE OF SPECIMENS #5-7

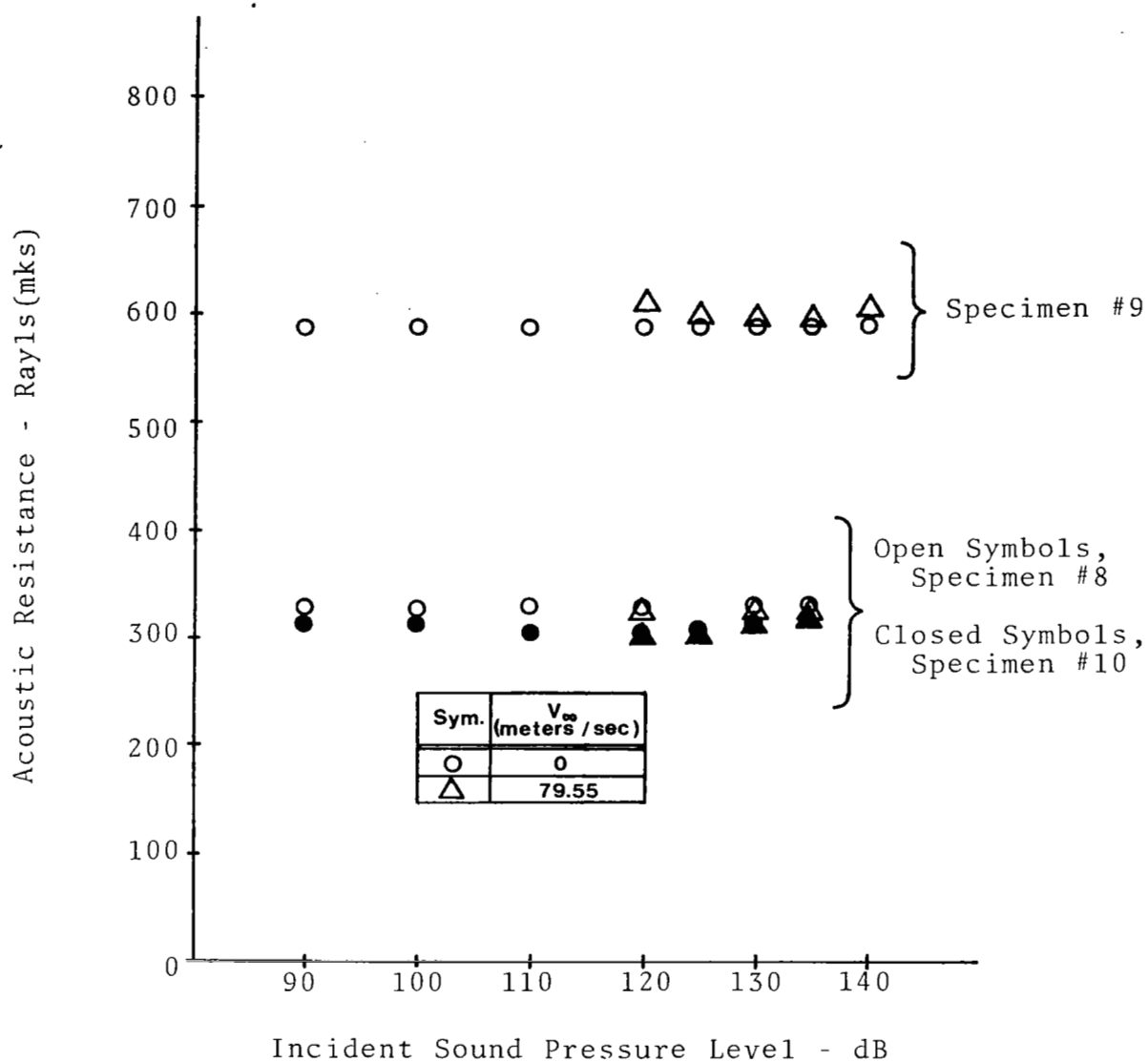


FIGURE 16. EFFECTS OF GRAZING FLOW AND SOUND PRESSURE LEVEL ON THE ACOUSTIC RESSITANCE OF SPECIMENS #8-10

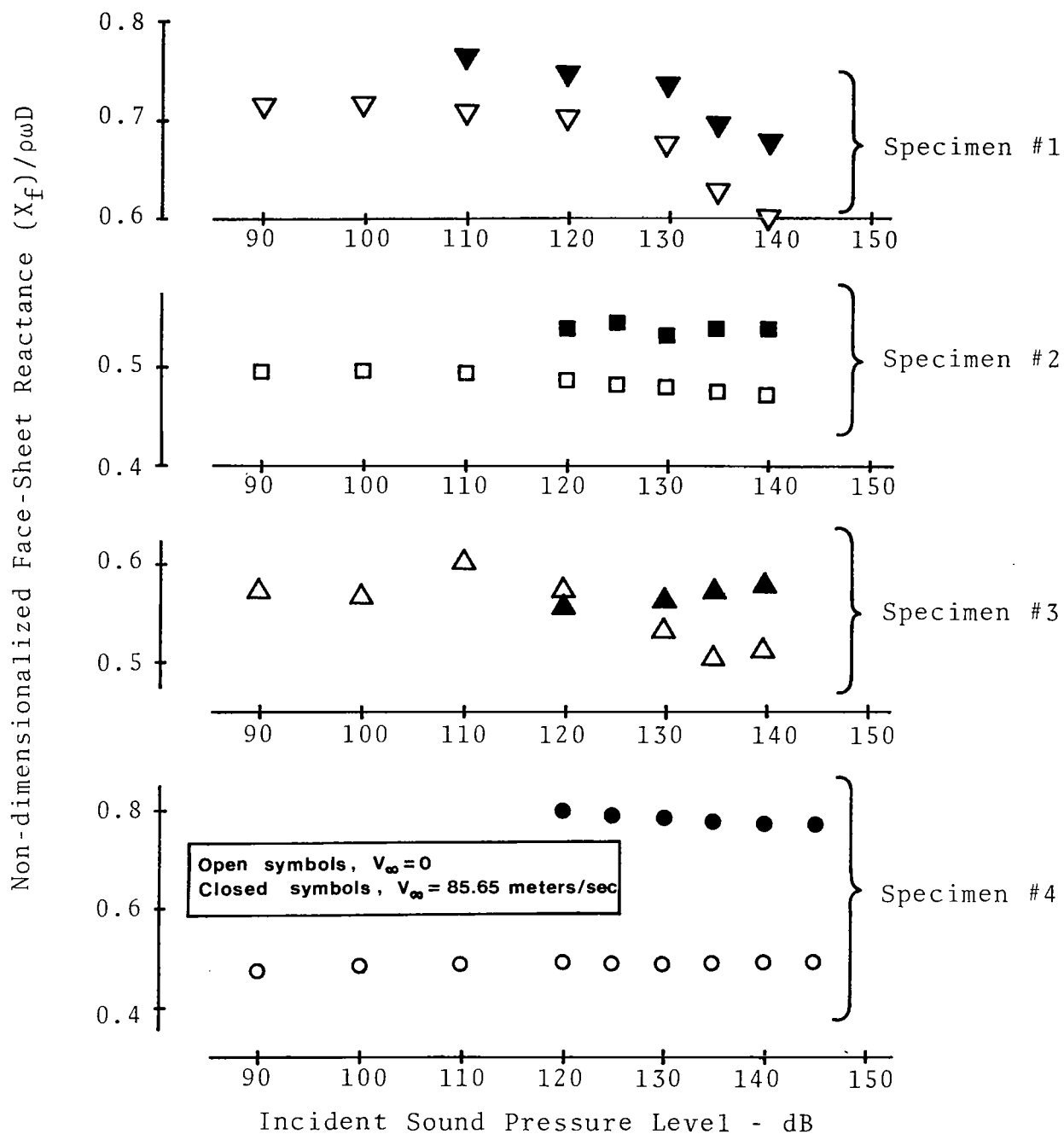


FIGURE 17. EFFECT OF GRAZING FLOW AND SOUND PRESSURE LEVEL ON FACE-SHEET REACTANCE OF SPECIMENS #1-4

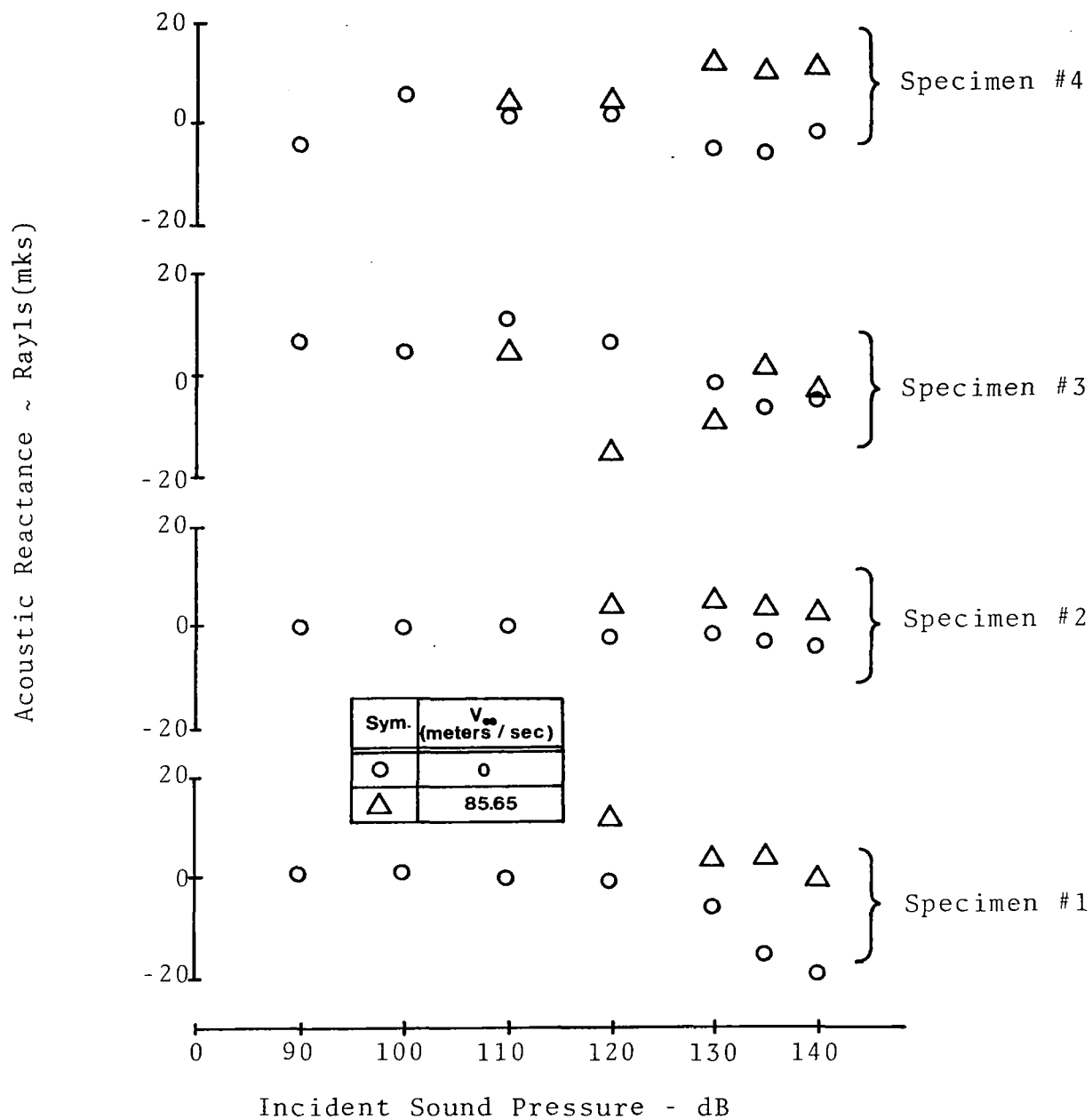


FIGURE 18. EFFECTS OF GRAZING FLOW AND SOUND PRESSURE LEVEL ON THE TOTAL REACTANCE OF SPECIMENS #1-4

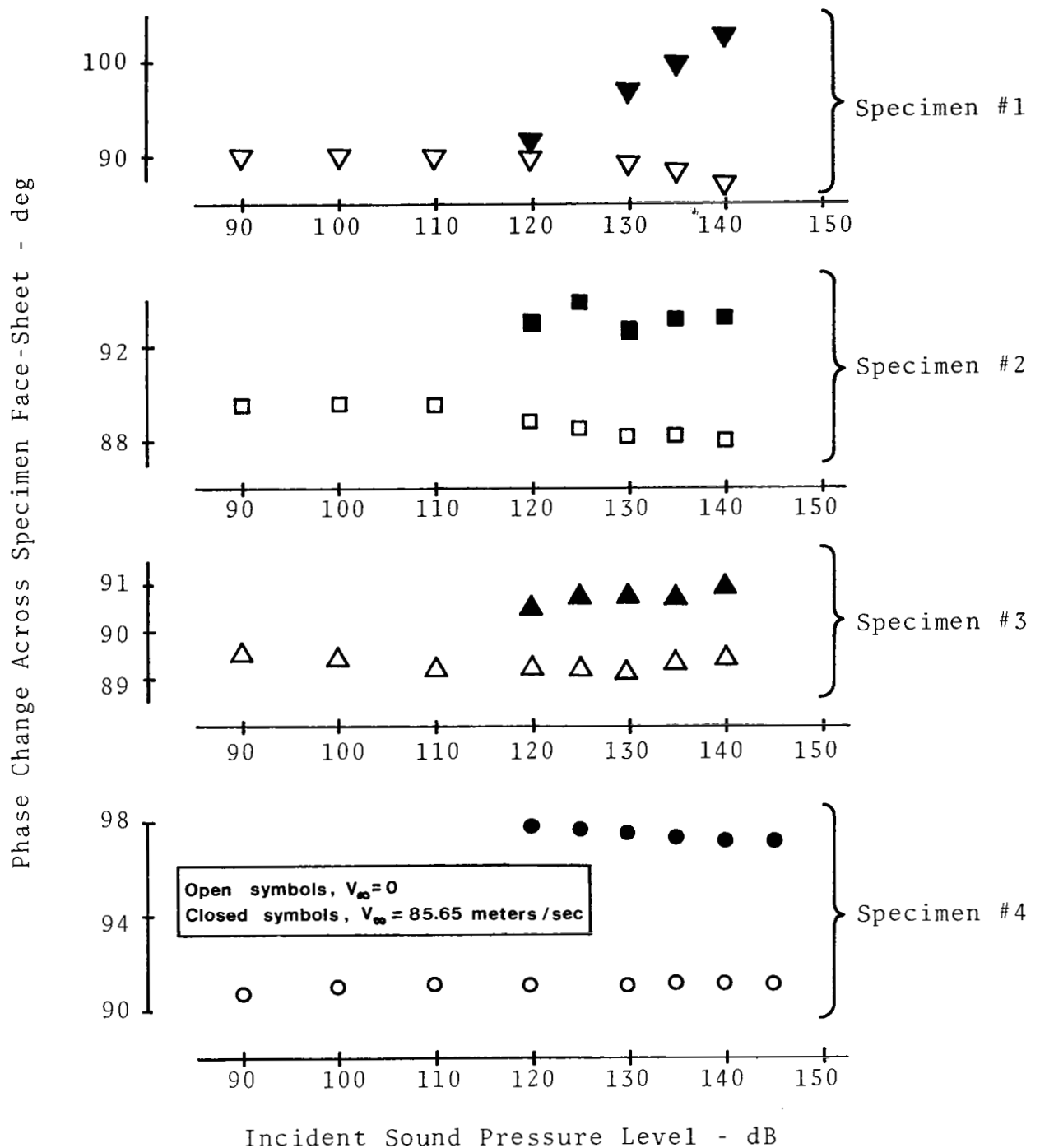


FIGURE 19. EFFECT OF GRAZING FLOW AND SOUND PRESSURE LEVEL ON PHASE ANGLE CHANGE ACROSS THE FACE-SHEET OF SPECIMENS #1-4

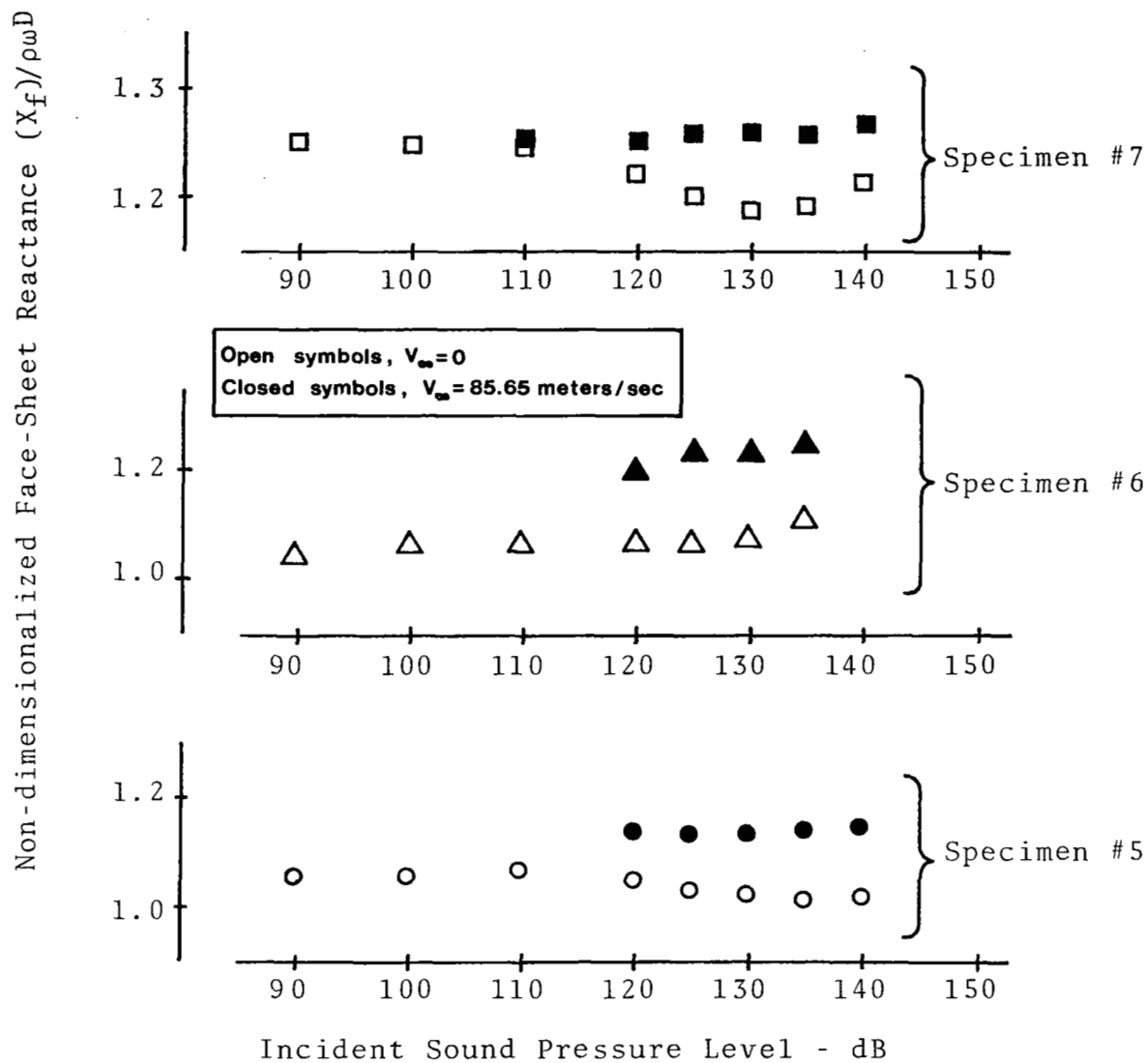


FIGURE 20. EFFECT OF GRAZING FLOW AND SOUND PRESSURE LEVEL ON FACE-SHEET REACTANCE OF SPECIMENS #5-7

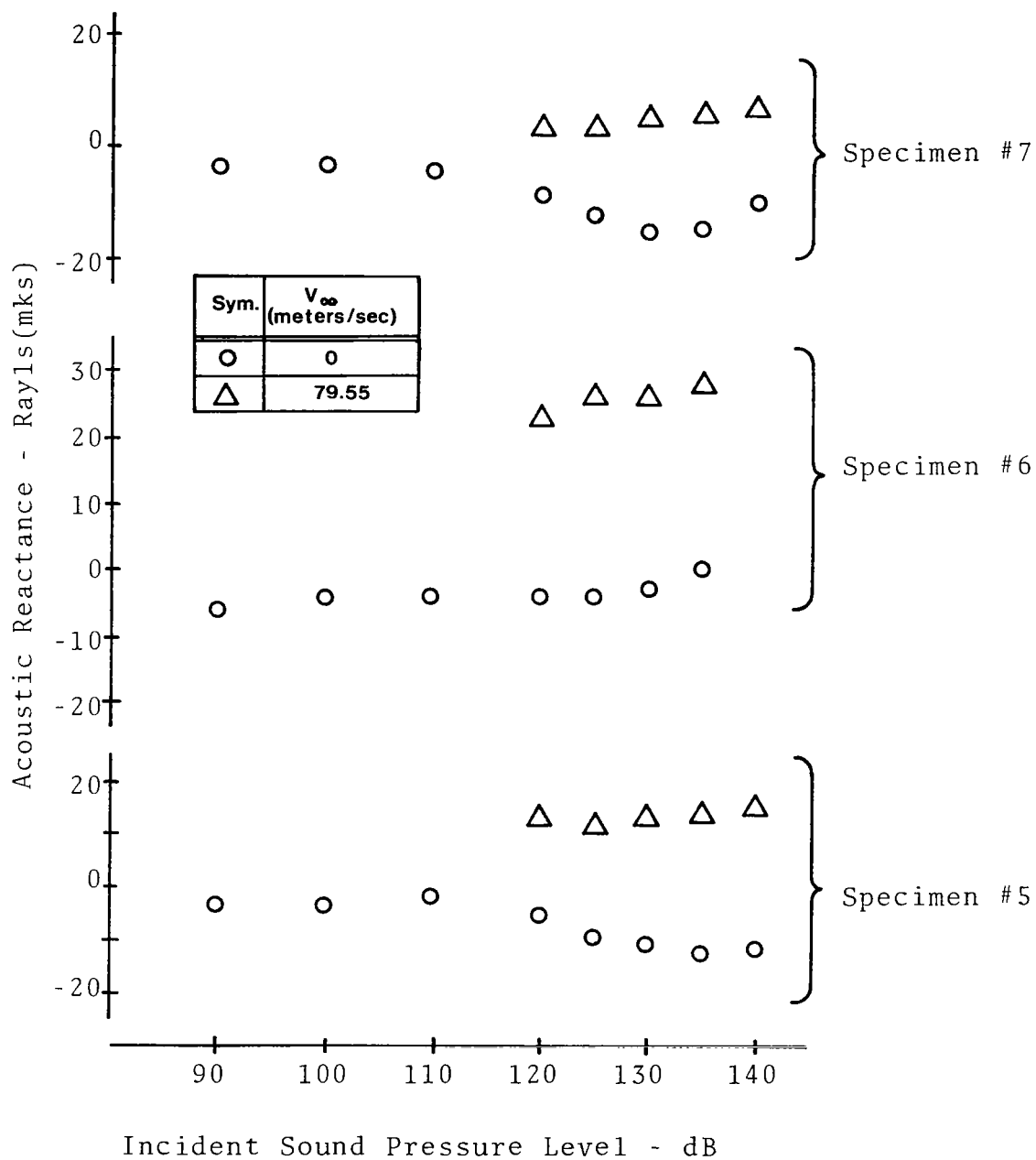


FIGURE 21. EFFECT OF GRAZING FLOW AND SOUND PRESSURE LEVEL ON THE TOTAL ACOUSTIC REACTANCE OF SPECIMENS #5-7

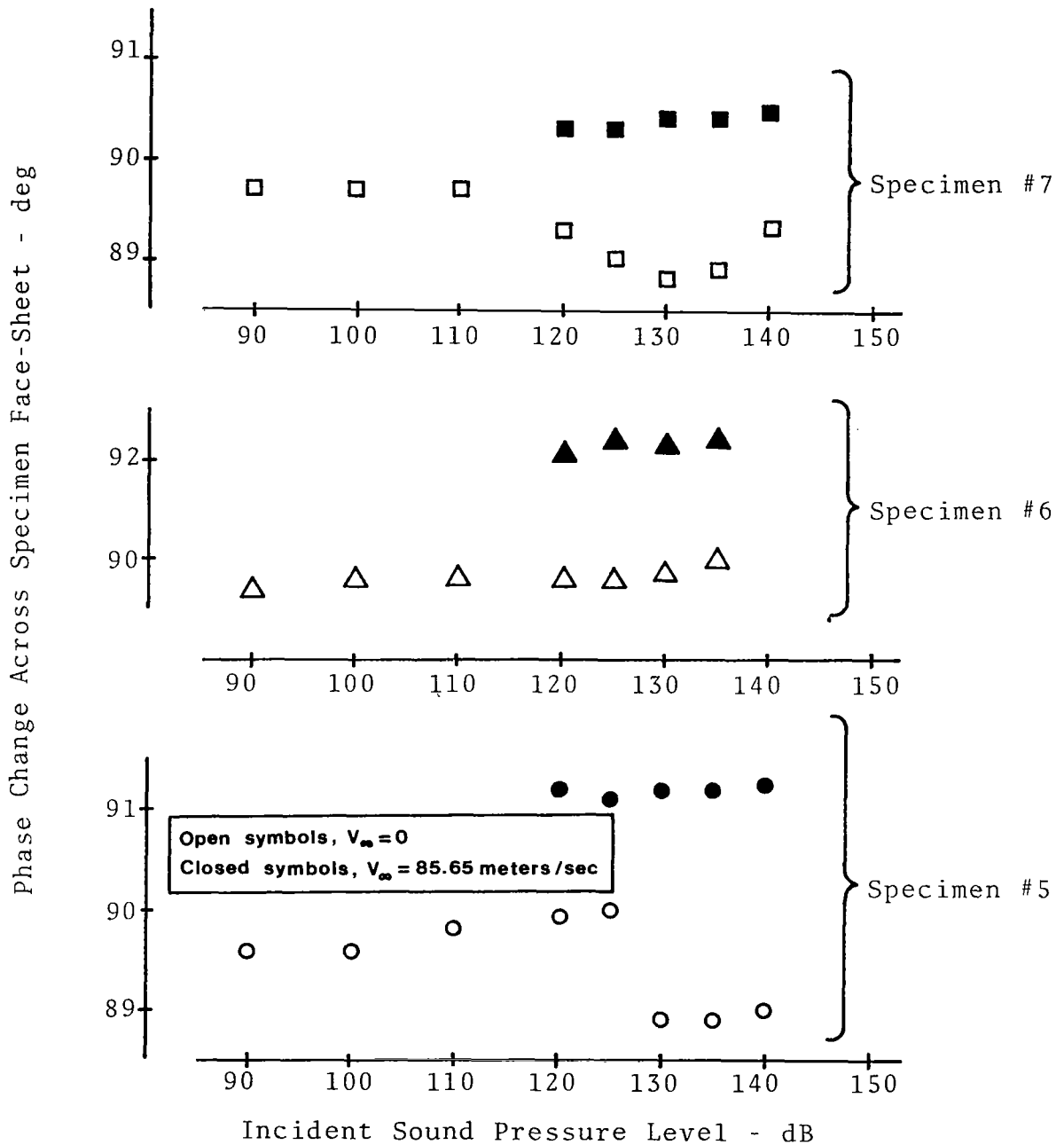


FIGURE 22. EFFECT OF GRAZING FLOW AND SOUND PRESSURE LEVEL ON THE PHASE ANGLE CHANGE ACROSS THE FACE-SHEET OF SPECIMENS #5-7

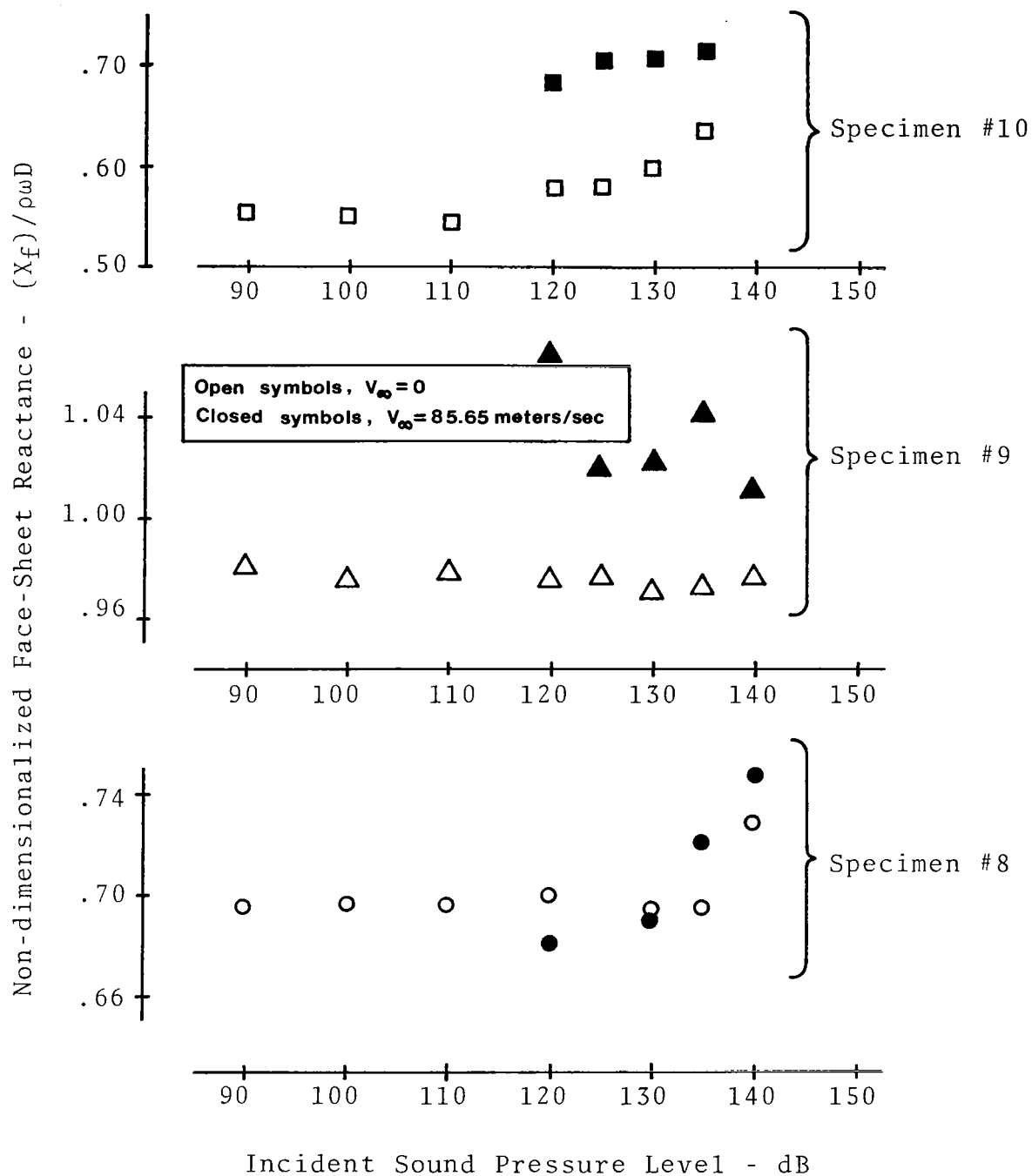


FIGURE 23. EFFECT OF GRAZING FLOW AND SOUND PRESSURE LEVEL ON THE FACE-SHEET REACTANCE OF SPECIMENS #8-10

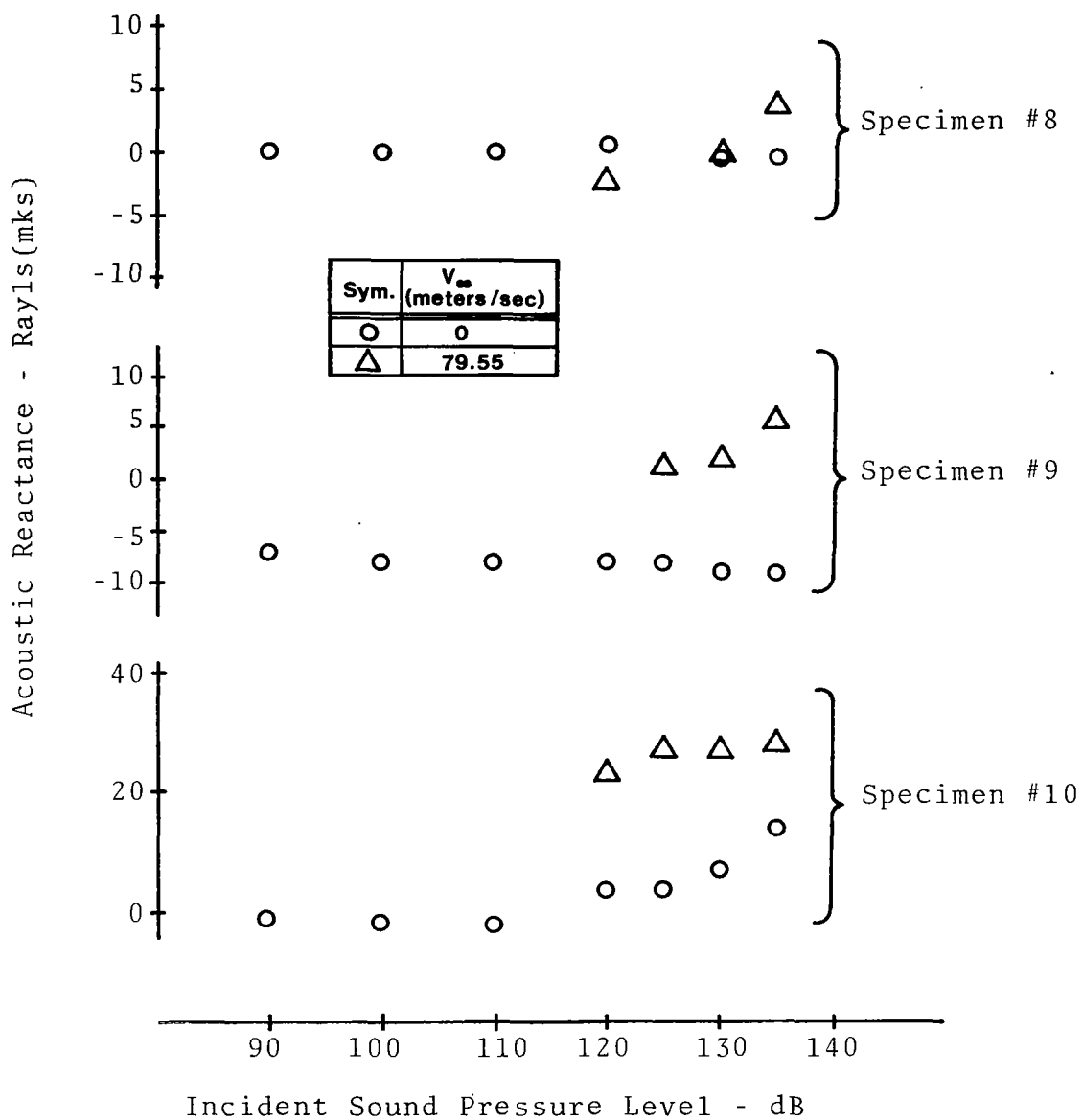


FIGURE 24. EFFECT OF GRAZING FLOW AND SOUND PRESSURE LEVEL ON THE TOTAL REACTANCE OF SPECIMENS #8-10

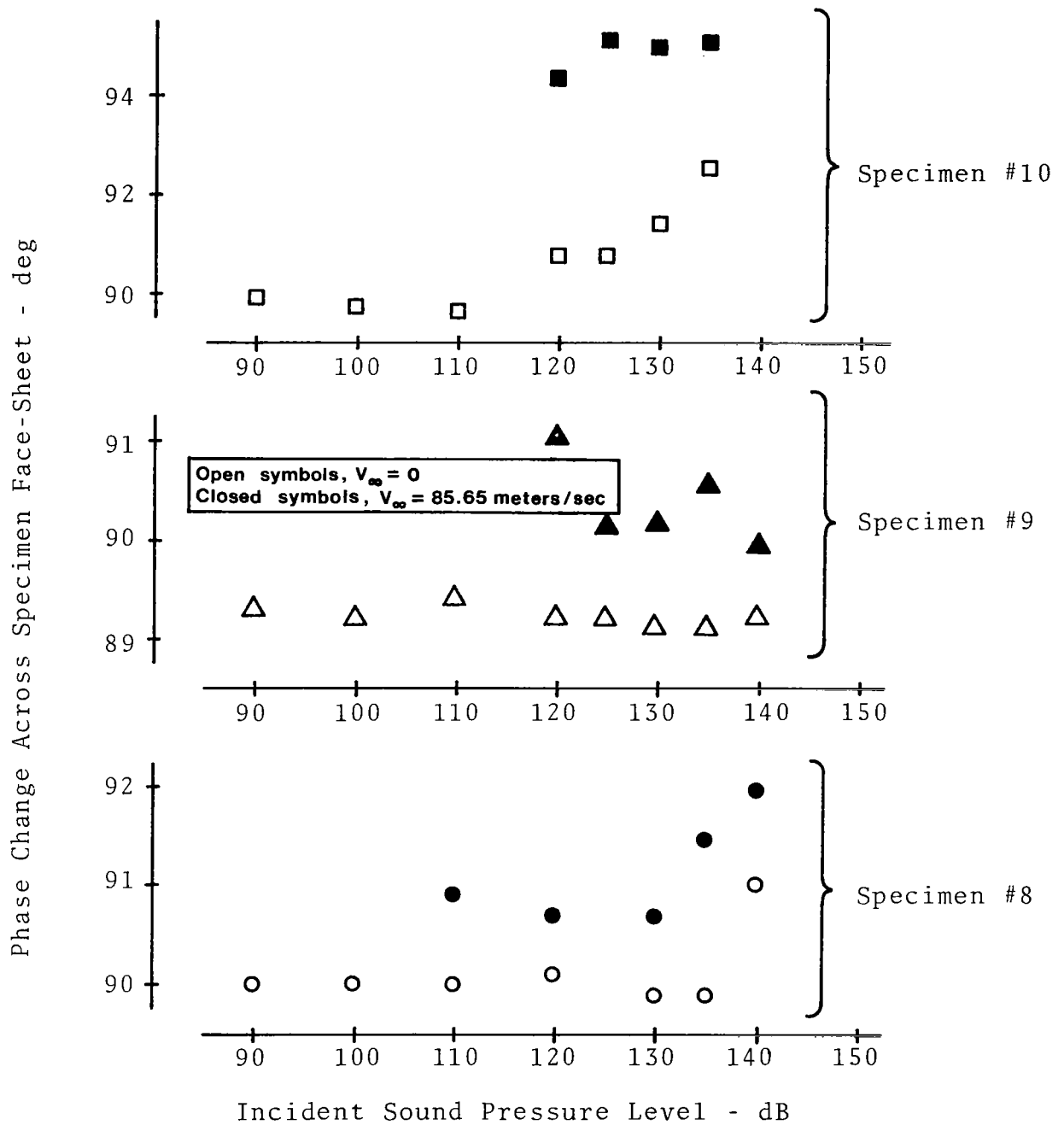


FIGURE 25. EFFECT OF GRAZING FLOW AND SOUND PRESSURE LEVEL ON PHASE ANGLE CHANGE ACROSS THE FACE-SHEET OF SPECIMENS #8-10

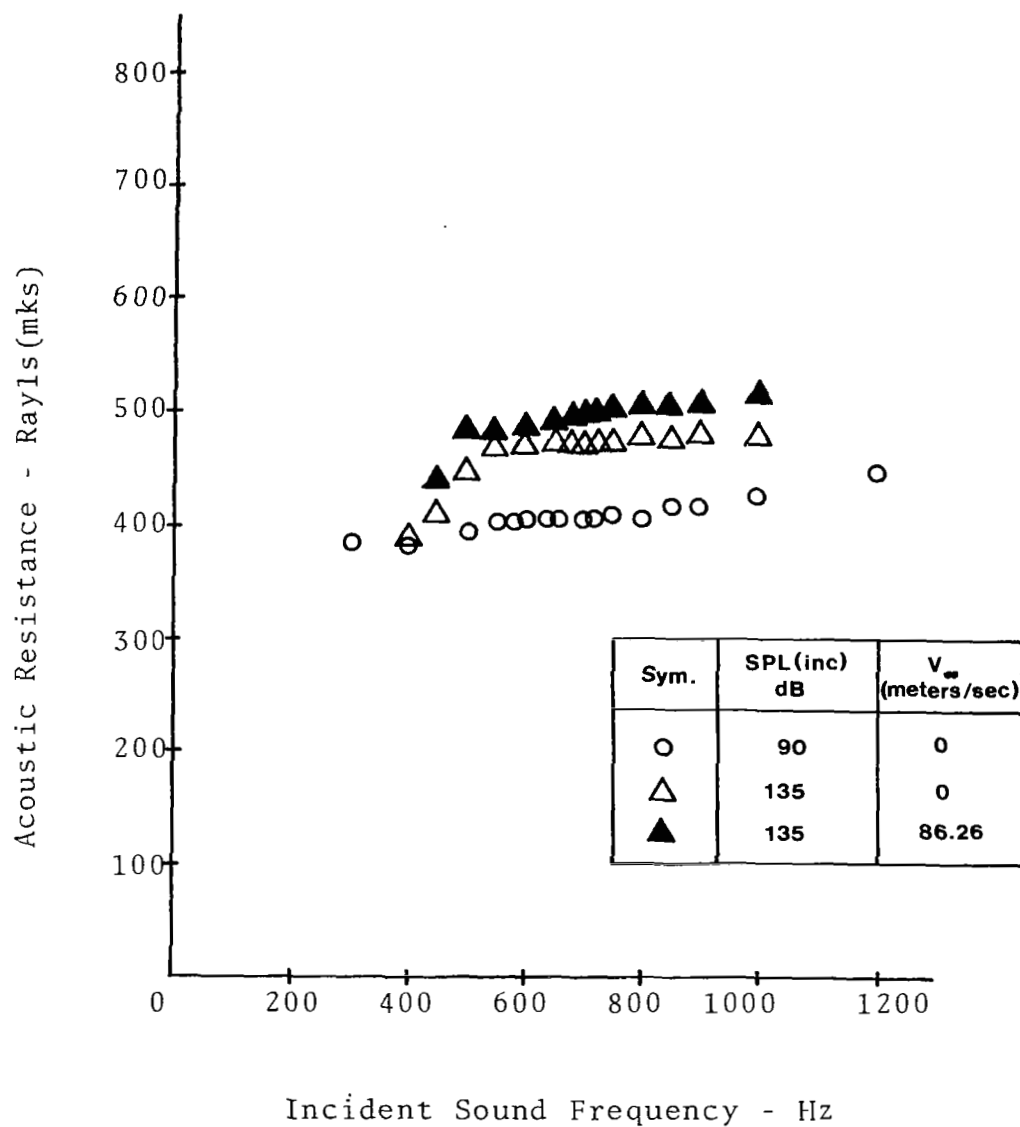


FIGURE 26. EFFECT OF VARIATION OF FREQUENCY ON THE ACOUSTIC RESISTANCE OF SPECIMEN #1

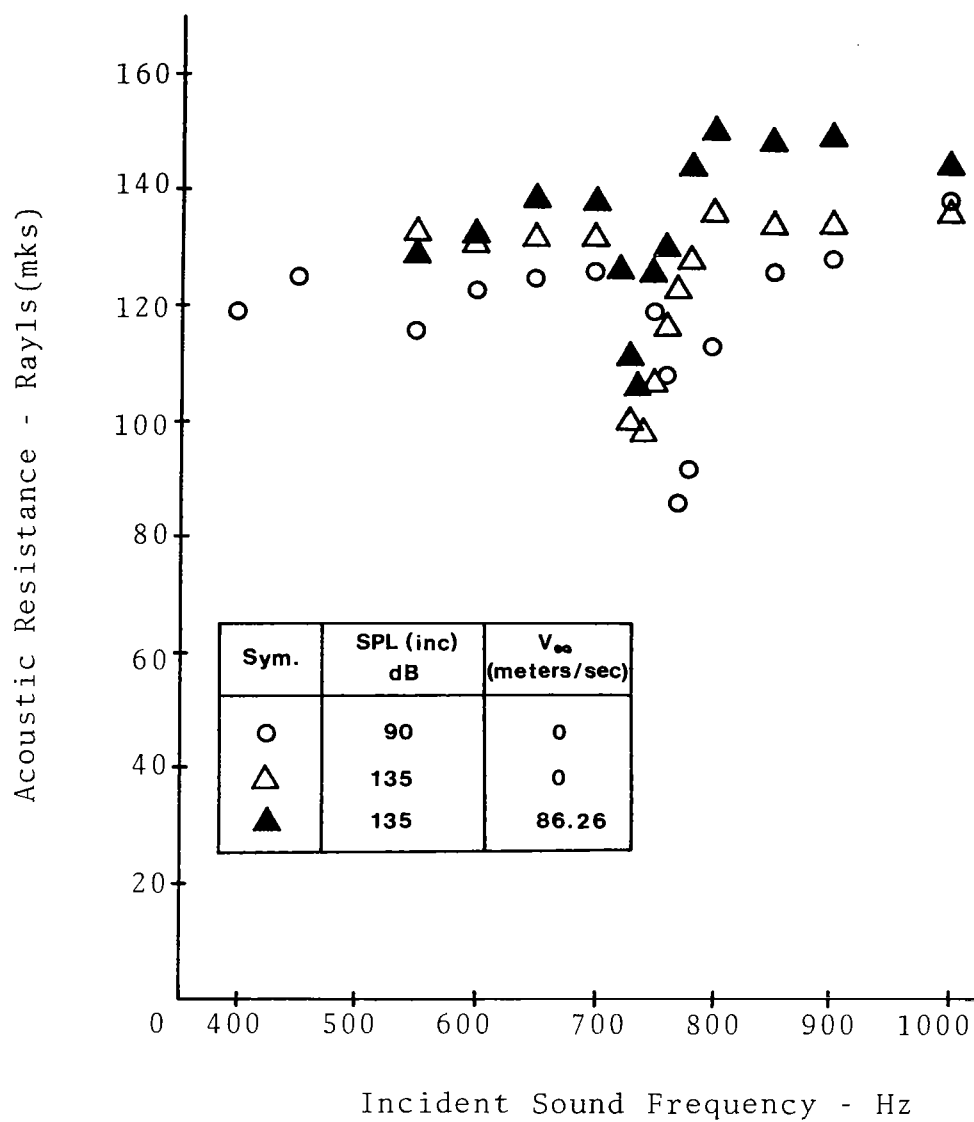


FIGURE 27. EFFECT OF VARIATION OF FREQUENCY ON THE ACOUSTIC RESISTANCE OF SPECIMEN #2

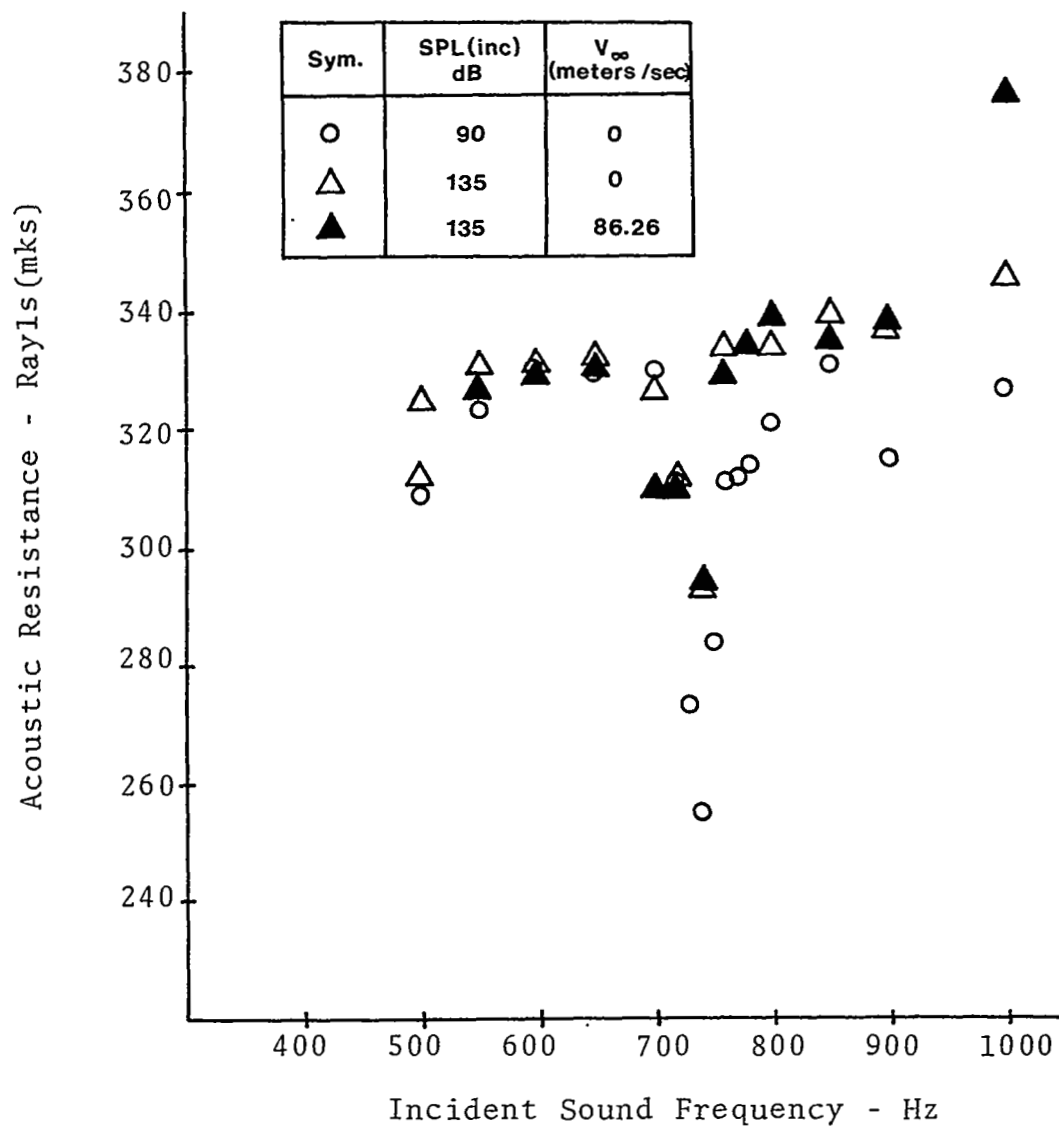


FIGURE 28. EFFECT OF VARIATION OF FREQUENCY ON THE ACOUSTIC RESISTANCE OF SPECIMEN #7

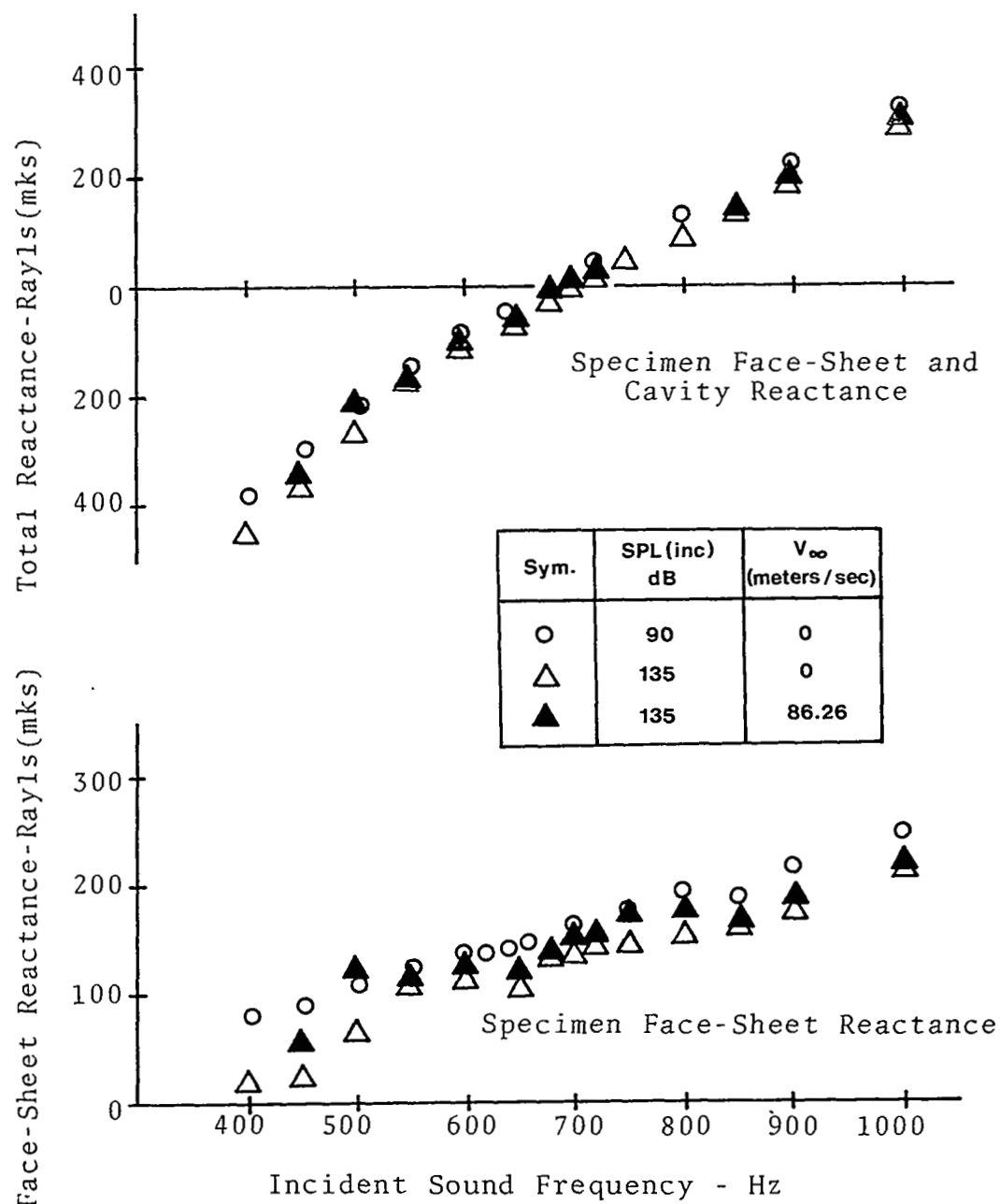


FIGURE 29. EFFECT OF VARIATION OF FREQUENCY ON THE ACOUSTIC REACTANCE OF SPECIMEN #1

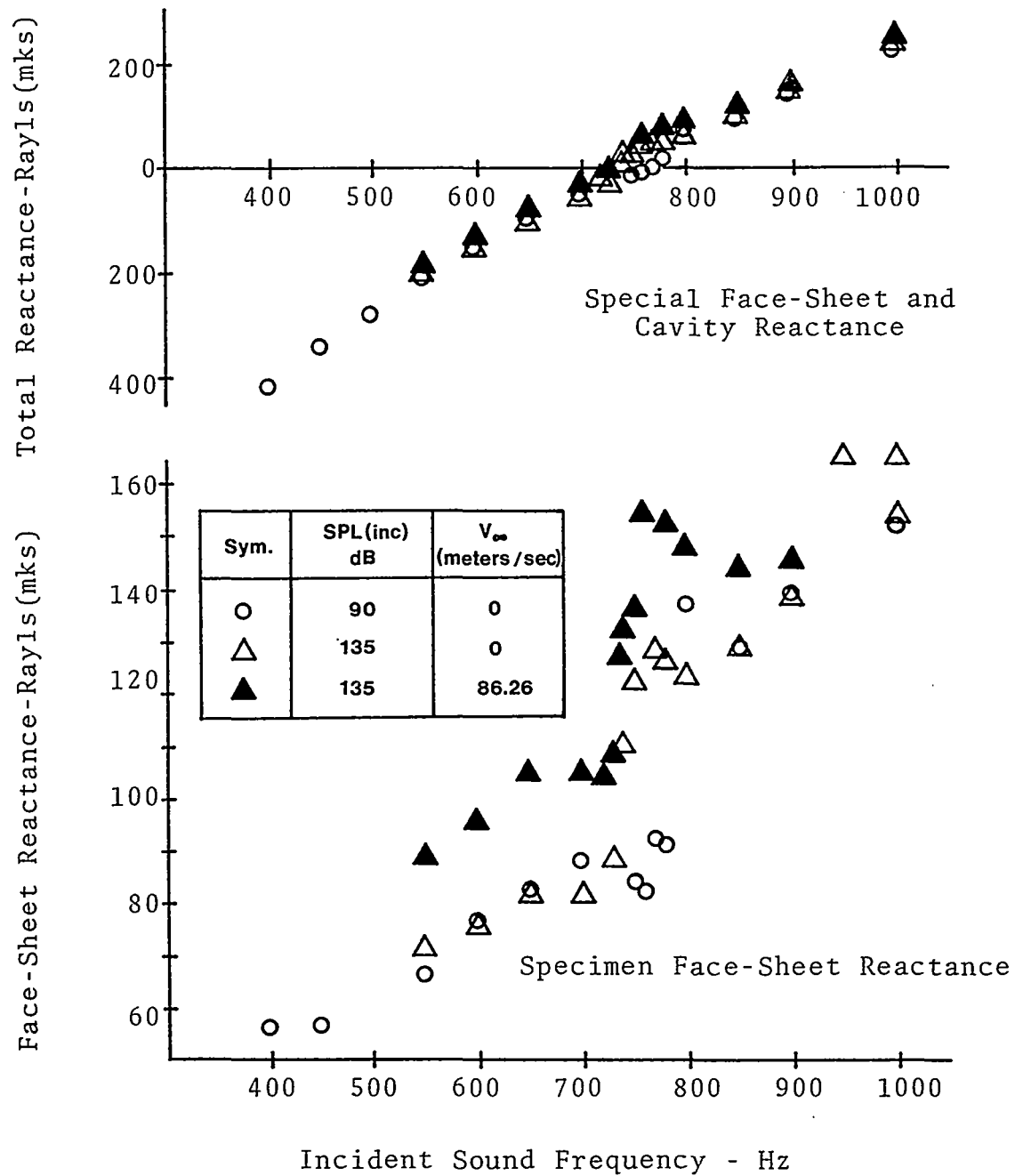


FIGURE 30. EFFECT OF VARIATION OF FREQUENCY ON THE ACOUSTIC REACTANCE OF SPECIMEN #2

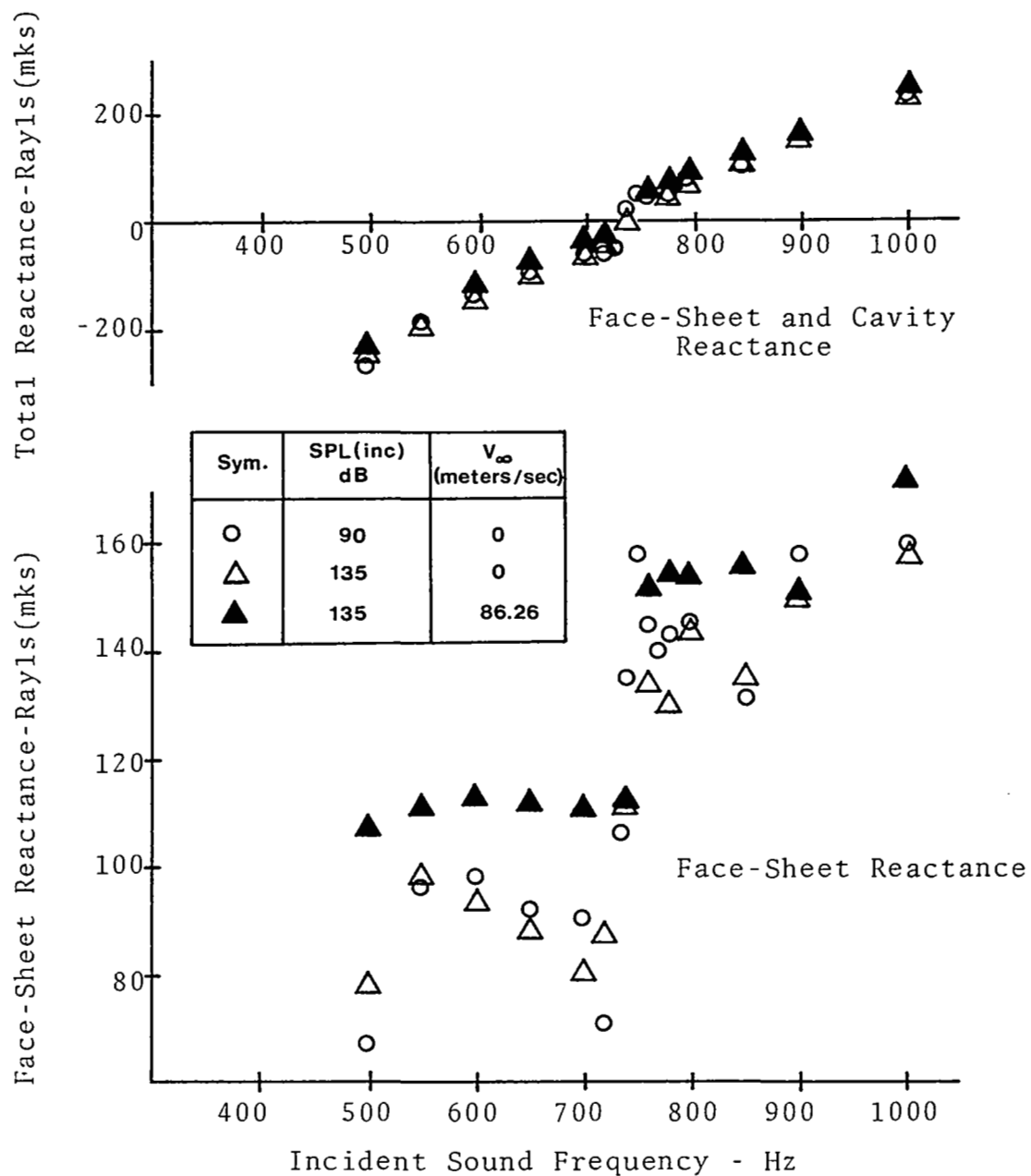


FIGURE 31. EFFECT OF VARIATION OF FREQUENCY ON THE REACTANCE OF SPECIMEN #7

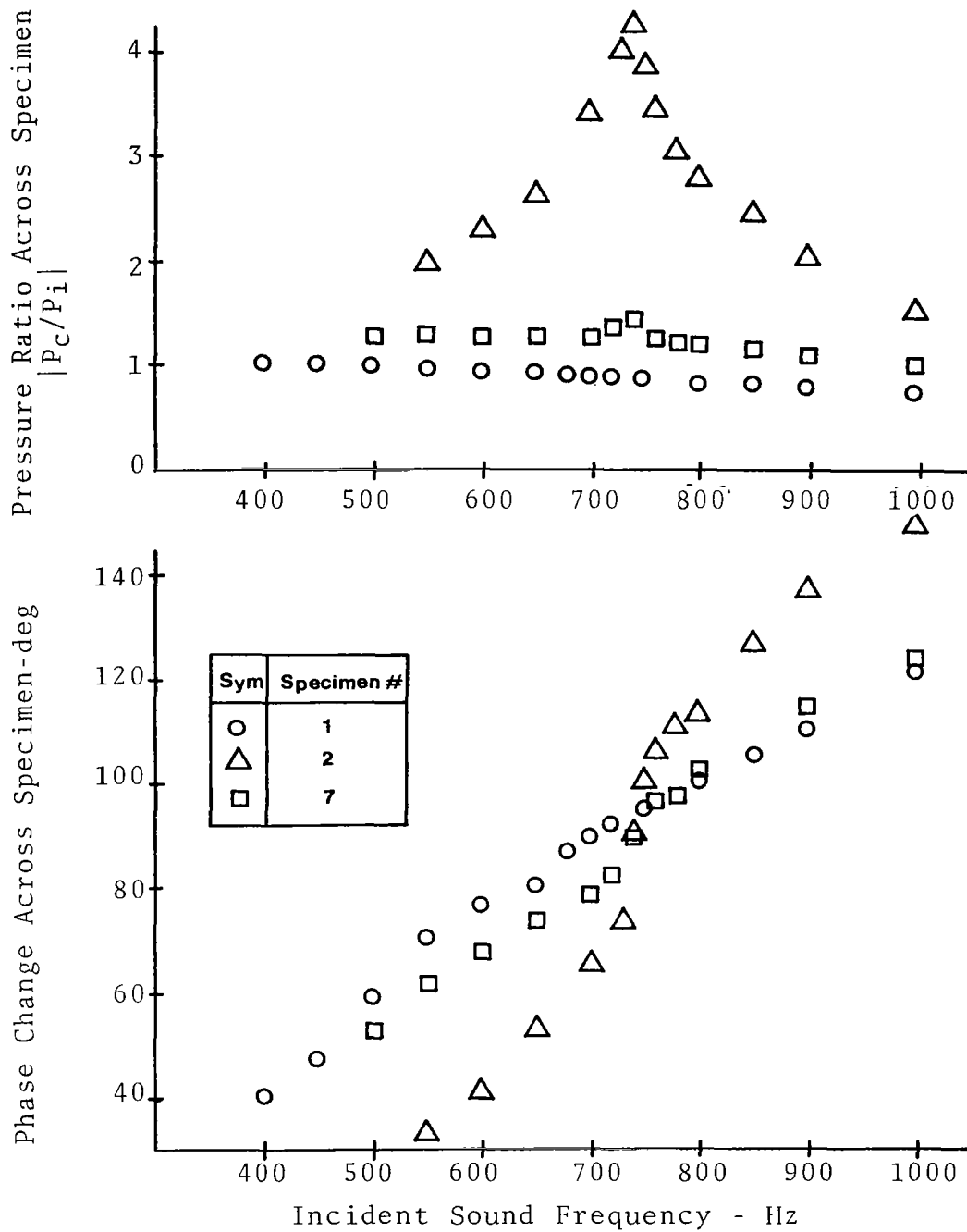


FIGURE 32. EFFECT OF FREQUENCY VARIATION ON THE PRESSURE RATIOS AND PHASE CHANGES ACROSS SPECIMENS 1, 2 & 7

APPENDIX A

CORRECTION TO MEASURED INCIDENT SOUND PRESSURE LEVEL DUE TO ACOUSTIC RADIATION FROM THE TEST SPECIMEN

To measure the acoustic impedance of a sheet of porous material backed by a cavity using the two-microphone method, it is necessary to accurately determine the difference in sound pressure level and phase between a microphone mounted flush with the surface of the test specimen and another mounted at the back of the resonator cavity. As has been pointed out in Section 4.1, it is necessary to mount the "incident" microphone sufficiently far from the test specimen so that it is not influenced by the hydrodynamic near field.

The typical behavior of highly resistive specimens was as follows. The frequency of the incident sound field was adjusted to resonance which corresponds to a relative phase across the specimen $\phi = 90$ degrees. During this adjustment the incident sound pressure level was set at 90 dB; ϕ was observed to decrease monotonically with increasing sound pressure level. This was the usual response of highly resistive porous specimens. However, for particularly low resistance specimens, ϕ was observed to initially increase by several degrees with increasing sound pressure level before decreasing. Additionally, it was noted that in the range of this anomalous phase behavior, increasing the drive level to the loudspeaker by 5 dB would result in somewhat greater than 5 dB increase in the measured incident sound pressure level.

This can be explained in terms of acoustic radiation from the test sample as follows: Let Q be the inward volume velocity in the orifice or porous sample, P_{cav} be the cavity sound pressure, P_{inc} be the incident sound pressure, $(Z_D) = (R_D) + (X_D)$ be the specific acoustic impedance of the sample, normalized to the cavity diameter D , L be the cavity depth, and r be the distance from the acoustic center of the specimen to the "incident" measuring location.

For sinusoidal excitation $P_{inc} = P_{inc} e^{i\omega t}$, where henceforth the $e^{i\omega t}$ will be assumed. We therefore have, for the volume velocity

$$Q = \frac{P_{inc}}{Z_D} \cdot \frac{\pi D^2}{4} \quad (A-1)$$

and from mass conservation and adiabatic compression,

$$P_{cav} \approx \frac{4\rho c^2}{\pi D^2 L} \int Q dt = -i \frac{4\rho c^2 Q}{\pi D^2 L \omega} \quad (A-2)$$

Combining Eqs. (A-1) and (A-2),

$$P_{cav} = \frac{P_{inc}}{Z_D} \frac{\rho c^2}{\omega L} e^{-i\pi/2} (Z_D = R_D + iX_D) \quad (A-3)$$

The radiated pressure P_r for a small source in a plane surface is given by

$$P_r(r) = -i \frac{\rho \omega Q}{2 \pi r} e^{-i \frac{\omega r}{c}} \quad (A-4)$$

Combining Eqs. (A-1) and (A-4)

$$P_r(r) = -i \frac{\rho \omega P_{inc} D^2}{Z_D \cdot 8r} e^{-i \omega r / c}$$

$$\frac{P_r(r)}{P_{inc}} = \frac{\rho \omega D^2}{8 Z_D \cdot r} e^{-i \left(\frac{\omega r}{c} + \pi/2 \right)} \quad (A-5)$$

Therefore, the total sound pressure P_t at the incident microphone will be given by

$$P_t = P_{inc} \left(1 + \frac{P_r(r)}{P_{inc}} \right) = P_{inc} \left[1 + \frac{\rho \omega D^2}{8r (R_D^2 + X_D^2)} (R_D - iX_D) e^{-i \left(\frac{\omega r}{c} + \frac{\pi}{2} \right)} \right] \quad (A-6)$$

Unfortunately, this otherwise convenient expression includes R_D and X_D , which we are attempting to measure, and an iterative calculation is required to correct for the effect. Transposing we have

$$P_{inc} = P_t \left[1 + \frac{\rho \omega D^2}{8r (R_D^2 + X_D^2)^{1/2}} e^{-i \left(\frac{\omega r}{c} + \frac{\pi}{2} + \arctan \frac{X_D}{R_D} \right)} \right]^{-1} \quad (A-7)$$

or

$$P_{inc} = P_t \left(1 + A^2 + 2A \cos B \right)^{-1/2} e^{i \arctan \left(\frac{A \sin B}{1 + A \cos B} \right)} \quad (A-8)$$

where

$$A = \frac{\rho \omega D^2}{8r (R_D^2 + X_D^2)^{1/2}} \quad (A-9)$$

and

$$B = \frac{\omega r}{c} + \frac{\pi}{2} + \arctan \left(X_D / R_D \right) \quad (A-10)$$

Thus,

$$SPL_i = SPL_t - 10 \log \left(1 + A^2 + 2A \cos B \right) \quad (A-11)$$

$$\phi_i = \phi_t + \arctan \left(\frac{A \sin B}{1 + A \cos B} \right)$$

The iterative calculation proceeds as follows:

1. Use $SPL_t - SPL_i$ and $\phi_t - \phi_i$ to determine on initial value of R_D and X_D .
2. Use these values of R_D and X_D in Eqs. (A-8) thru (A-11) to determine a first iteration value of SPL_i and ϕ .

3. Calculate new values of R_D and X_D .
4. Repeat steps 2 and 3 until the answers from two successful iterations are equal within the desired accuracy (0.1% requires only 3-4 iterations).

Results of this correction procedure for low sound pressure level data from porous samples 1 through 10 are shown in Table A-1. Note that for each case, ΔSPL is lower than measured, ϕ is higher than measured, $R/\rho c$ is slightly higher than measured and $X/\rho c$ is more positive than measured.

TABLE A-1 SUMMARY OF CORRECTED IMPEDANCES TO TEN POROUS SPECIMENS

$$V_{\infty} = 0; \text{SPL(inc)} = 90 \text{ dB}$$

Sample #	Meas ΔSPL (dB)	Meas ϕ_{ic} (deg)	Init $R/\rho c$	Init $X/\rho c$	Corr ΔSPL (dB)	Corr ϕ_{ic} (deg)	Corr $R/\rho c$	Corr $X/\rho c$
1	.58	90.1	.9794	.0017	.37	92.3	1.0026	.0397
2	10.07	90.0	.3219	.0000	9.35	96.47	.3474	.0394
3	-6.90	90.4	2.2791	.0159	-7.00	91.37	2.3045	.0551
4	-4.01	90.0	1.6503	.0000	-4.26	91.53	1.6983	.0455
5	- .82	89.9	1.2453	-.0022	-1.03	91.75	1.2748	.0389
6	-1.84	89.9	1.3400	-.0023	-1.97	91.41	1.3595	.0335
7	-3.02	89.8	1.6500	-.0058	-3.16	91.17	1.6770	.0342
8	2.83	90.1	.7773	.0014	2.60	92.68	.7971	.0373
9	7.63	90.0	.4725	.0000	7.01	94.82	.5059	.0427
10	5.56	89.7	.5621	-.0029	5.23	93.30	.5829	.0336

1. Report No. NASA CR-2951		2. Government Accession No.		3. Recipient's Catalog No.	
4. Title and Subtitle Effects of Grazing Flow on the Steady-State Flow Resistance and Acoustic Impedance of Thin Porous-Faced Liners				5. Report Date January 1978	
				6. Performing Organization Code	
7. Author(s) A. S. Hersh & B. Walker				8. Performing Organization Report No.	
				10. Work Unit No.	
9. Performing Organization Name and Address Hersh Acoustical Engineering 9545 Cozycroft Avenue Chatsworth, CA 91311				11. Contract or Grant No. NAS1-14310	
				13. Type of Report and Period Covered Contractor Report	
12. Sponsoring Agency Name and Address National Aeronautics and Space Administration Washington, DC 20546				14. Sponsoring Agency Code	
15. Supplementary Notes Final Report, Project Manager, Tony L. Parrott, Acoustics Branch, Acoustics and Noise Reduction Division, NASA Langley Research Center, Hampton, VA 23665					
16. Abstract <p>The results of an investigation of the effects of grazing flow on the steady-state flow resistance and acoustic impedance of seven Feltmetal and three Rigimesh thin porous-faced liners are presented. A state-of-the-art review of previous nongrazing flow studies is also presented. The steady-state flow resistance of the ten specimens are measured using standard fluid mechanical experimental techniques. The acoustic impedance was measured using the two-microphone method. The principal findings of the study are (1) the effects of grazing flow were measured and found to be small, (2) small differences were measured between steady-state and acoustic resistance, (3) a semi-empirical model was derived that correlated the steady-state resistance data of the seven Feltmetal liners and the face-sheet reactance of both the Feltmetal and Rigimesh liners.</p> <p>These findings suggest that nongrazing flow steady-state flow resistance tests could provide considerable insight into the acoustic behavior of porous liners in a grazing flow environment.</p>					
17. Key Words (Suggested by Author(s)) Acoustic Impedance Grazing Flow Effects Measurements			18. Distribution Statement Unclassified - unlimited STAR Category 71		
19. Security Classif. (of this report) Unclassified	20. Security Classif. (of this page) Unclassified	21. No. of Pages 78	22. Price* \$6.00		